Acta Geochim (2024) 43:904–932
https://doi.org/10.1007/s11631-024-00679-1

ORIGINAL ARTICLE

Mineralogy and whole-rock geochemistry of the Oligocene Barail Group of rocks of Belt of Schuppen, Northeast India: Implications for tectono-provenance and paleo-weathering

Manash Pratim Gogoi[1] · Yunpeng Dong[2] · Pradip Borgohain[1] · Devojit Bezbaruah[3] · Arvind Pandey[4] · Yadav Krishna Gogoi[1] · Garima Konwar[1] · Gautam Raj Bawri[5] · Bubul Bharali[6]

Received: 11 June 2023 / Revised: 7 January 2024 / Accepted: 31 January 2024 / Published online: 14 March 2024

Abstract The petrographic and geochemical attributes of the Oligocene Barail Group of rocks are used to decipher the likely source area(s) or tectonic domains, as this sequence of rocks was deposited in a foreland basin governed by orogenic domain, namely the North-east Arunachal Himalayas. The river system that gave rise to the Brahmaputra River (Yarlung-Tsangpo), which flowed through several tectonic domains of the Himalayan ranges, primarily from Bomi-Chayu, Gangadese Granitoid, Higher Himalayan Leucogranites, and Namche Barwa into the proto Bengal Basin now a part of Assam Arakan Basin and Naga Schuppen Belt, was the main source of the sandstone formation of the Barail Group. The purpose of sandstone petrography, which combines modal analysis with XRF (Major Oxides) and HR-ICP-MS (Trace & Rare Earth Elements) research, is to identify the type of source rock(s), their weathering pattern, and its paleo-environmental circumstances. These sandstones were formed from recycled orogen and include lithic and sublithic arenite variants with advanced texture and chemical maturity. The sediments were felsic (Th/Co: 1.38, Cr/Th: 9.78, La/Lu: 11.58, Th/Sc: 0.99, Eu/Eu*: 0.66, La/Sc: 3.05, La/Co: 4.18), with contributions from intermediate source rocks and low-rank metamorphics deposited in an active continental margin to a continental island arc setting. Climatic conditions impacted the sediments of Barails, characterised by being warm and semi-humid to humid which resulted in moderate to a high degree of chemical weathering, as shown by weathering indices like CIA (79.14), PIA (85.47), CIW (86.9), WIP (32.50), ICV (0.71), and Th/U (6.03), which were further additionally supported by C-Value (1.01), PF (1.20), Sr/Cu (2.04), and Rb/Sr (0.97).

Keywords Belt of Schuppen · Barail Group · Sandstone · Petrography · Geochemistry · Provenance · Tectonic setting

1 Introduction

The study of provenance aids in determining the type of source area, lithologies, variables of the tectonic settings, and sedimentary history (Dickinson et al. 1983; Basu et al. 1975). The petrographic study provides clues to the probable source rocks, the tectonic setting, and the climatic condition of the source area. The main objective of the petrographic analysis is to understand in detail the mineralogical constituents, textural properties, diagenetic alterations, and their effect on the reservoir property of the sandstones. However, the petrography also provides information on the nature of source rocks and tectono-provenance settings. Geochemical compositions can also be utilized to determine the tectonic setting, provenance, and paleo-weathering conditions that

Supplementary Information The online version contains supplementary material available at https://doi.org/10.1007/s11631-024-00679-1.

✉ Bubul Bharali
bubulearth@gmail.com

[1] Department of Petroleum Technology, Dibrugarh University, Assam 786004, India

[2] Department of Geology, Northwest University, Xi'an 710069, China

[3] Department of Applied Geology, Dibrugarh University, Assam 786004, India

[4] Department of Statistics, Central University of Rajasthan, Ajmer 305817, India

[5] Department of Geology, Mizoram University, Aizawl, Mizoram 796004, India

[6] Department of Geology, Pachhunga University College, Aizawl, Mizoram 796001, India

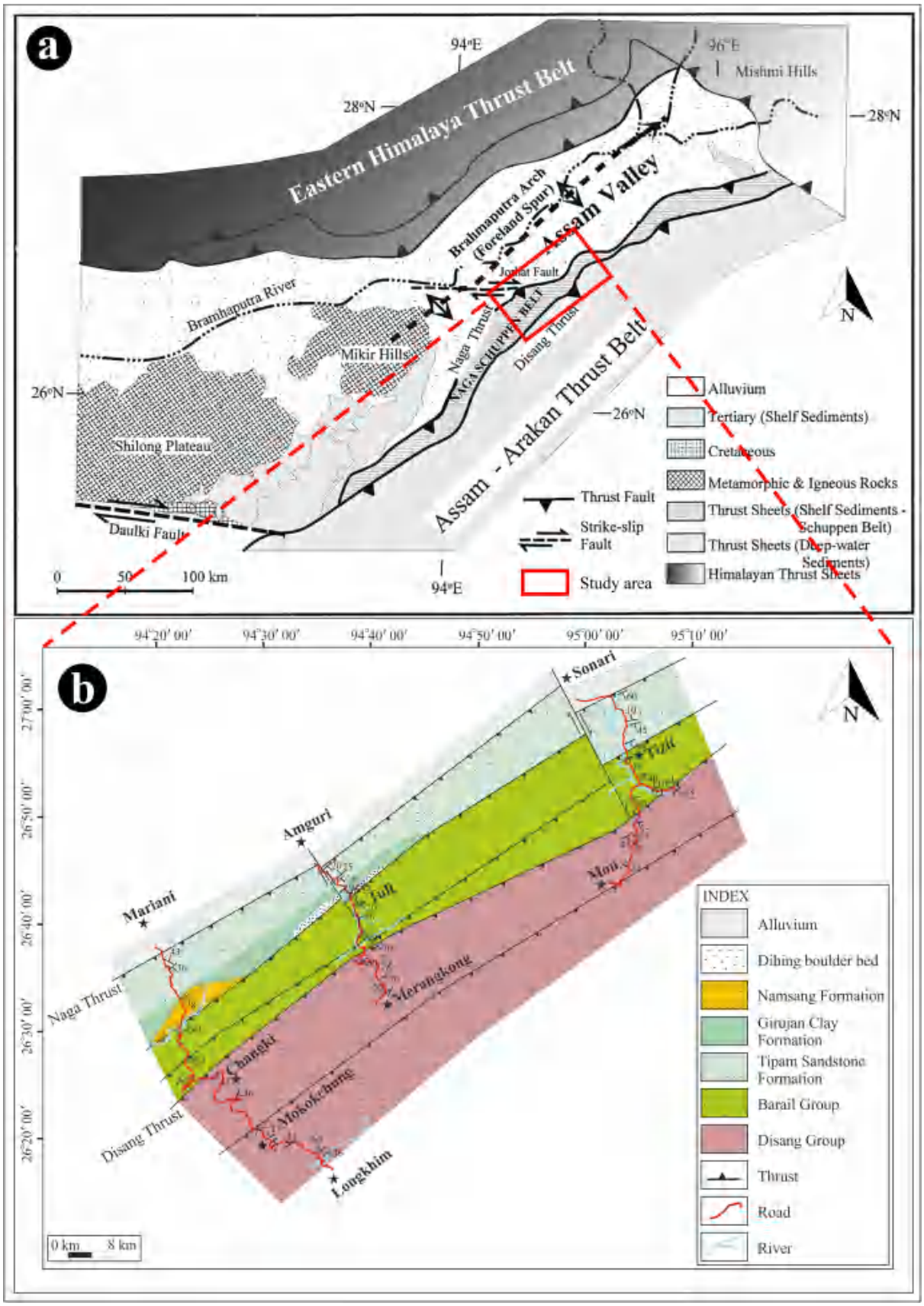
a
94°E
96°E
Mishmi Hills
28°N
Eastern Himalaya Thrust Belt
Brahmaputra Arch (Foreland Spur)
Assam Valley
Jorhat Fault
Bramhaputra River
Naga Thrust
NAGA SCHUPPEN BELT
Disang Thrust
Mikir Hills
26°N
Shilong Plateau
Assam - Arakan Thrust Belt
Daulki Fault
0 50 100 km
Alluvium
Tertiary (Shelf Sediments)
Cretaceous
Metamorphic & Igneous Rocks
Thrust Sheets (Shelf Sediments - Schuppen Belt)
Thrust Sheets (Deep-water Sediments)
Himalayan Thrust Sheets
Thrust Fault
Strike-slip Fault
Study area
N
b
94°20' 00'
94°30' 00'
94°40' 00'
94°50' 00'
95°00' 00'
95°10' 00'
27°00' 00'
26°50' 00'
26°40' 00'
26°30' 00'
26°20' 00'
Sonari
Tizit
Amguri
Mariani
Tuli
Mon
Naga Thrust
Merangkong
Changki
Mokokchung
Disang Thrust
Longkhim
0 km 8 km
INDEX
Alluvium
Dihing boulder bed
Namsang Formation
Girujan Clay Formation
Tipam Sandstone Formation
Barail Group
Disang Group
Thrust
Road
River

◂**Fig. 1** **a** Tectonic map of Assam-Arakan Basin showing the Belt of Schuppen (modified after Kent et al. 2002), **b** geological map prepared covering the three studied sections

prevailed during sedimentation. The chemical and mineralogical composition of clastic sedimentary rocks is controlled by the composition of their source rocks, environmental parameters influencing the weathering of the source rocks, duration of weathering, transportation mechanisms of clastics, and post-depositional processes. Therefore, the geochemistry of sedimentary rocks reflects a combination of provenance, chemical weathering, hydraulic sorting, and abrasion (Taylor and McLennan 1985; Wronkiewicz and Condie 1987; McLennan et al. 1993; Condie 1993; Nesbitt et al. 1997). The immobile major and trace elements carried in the sediment load have been valuable indicators of source terrain, weathering, tectonic, and environmental evolution (Taylor and McLennan 1985; Roser and Korsch 1988; Cullers 2000). Some trace elements, including rare earth elements (REEs), are relatively insoluble, and as a result, their original compositions remain unchanged during the sedimentary processes.

The Belt of Schuppen of Northeast India has piqued the curiosity of geoscientists for its complicated structure and tectonics, as well as the availability of crude oil and coal resources. The Barail (Oligocene) and Tipam (Miocene) Group of rocks, which are prolific producers of oil and gas in the Upper Assam Petroliferous Basin, are well exposed in neighbouring Schuppen Belt of Nagaland. However, there is little information about the mineralogy and tectono-provenance characteristics of the outcropped litho units of Naga Schuppen Belt. Moreover, the available literature shows that the subsurface Barail sandstones are different in many places of the outcropped area of Naga Schuppen Belt (Borgohain et al. 2021). Considering this view in mind, an attempt has been made in the present study to understand the provenance, tectonic settings, and paleo-weathering conditions that existed during the deposition of the Barail Group of sediments within the Belt of Schuppen, Northeast India by using petrography and whole-rock geochemistry.

2 Geology of the study area

Nagaland lies between 25°6'–27°4'N latitudes and 93°20′–95°15'E longitudes. The Belt of Schuppen is an imbricately faulted and thrusted belt of Cenozoic sediments forming the southeastern limit of Brahmaputra plain and separated from Patkai synclinorium by the Disang thrust. It covers approximately 200 km of the western margin of Nagaland state, trending in NE-SW directions. Paleogene and Neogene rocks are well exposed in the belt and are intensely folded and thrusted by a number of thrusts. The north-westernmost thrust is called the Naga thrust, while the south-easternmost thrust is known as the Disang thrust. Due to a complex geologic setup and some logistic issues, the Belt of Schuppen is poorly explored. Although a few earlier workers like Ranga et al. (1969), Thong (1999), Kent and Dasgupta (2004), Srivastava (2011), Borgohain et al. (2021), Bhuyan et al. (2022) and Gogoi et al. (2023) have done significant works on the Belt of Schuppen, especially on structure and tectonics, yet there are limited publications on geochemical aspects of the outcropped Paleogene rocks of the Belt of Schuppen. The present study area encompasses part of the Belt of Schuppen, Northeast India (Fig. 1a) along Sonari-Tizit-Mon (N27°00.975' E94°59.540' and N27°43.940' E95°04.163'), Amguri-Tuli-Merangkong (N26°43.619' E94°37.101' and N26°30.615' E94°40.186') and Mariani-Changki-Longkhim (N26°37.269' E94°20.647' and N26°18.091' E94°35.287') sections, where the Barail Group of rocks are exposed (Fig. 1b). The stratigraphic succession of the study area is shown in Table S1.

The Barail Group within the Belt of Schuppen consists mainly of alternate beds of sandstone and shale with minor coal seams at some places. The lower part of the Barail Group is mostly sandstone-dominated (Fig. 2a), while the upper part consists of alternate beds of sandstone and shale with coal seams (Fig. 2b). The sandstones are hard and compact, medium to fine-grained, and light grey. While the shales are dark grey to black, carbonaceous (Fig. 2c), and show well partings. Cross laminations (Fig. 2d), current ripples (Fig. 2e), small-scale channels, scour, and fill and slump structures are observed in the study area. A significant boulder bed consisting of rounded and elongated pebbles and boulders (Fig. 2f) with carbonaceous wood and coal streaks is observed within the Barail Group. This fan deposit is overlain by alternate beds of medium-grained sandstone with subordinate shale bands of Barail Group. A representation of the outcropped litho-columns of the studied sections is shown in Fig. 3.

3 Materials and methodology

Thirty-six (36) representative sandstone samples of Barail Group exposed along the study area have been considered for petrographic analysis. The petrographic study was carried out on rock thin sections prepared from air-dried, Araldite-impregnated samples using Leica-DM750P Trinocular Polarizing Microscope fitted with CCD camera and Leica Application Suite (LAS). The modal count was done by counting 500 points per thin section following Gazzi-Dickinson (1966) method.

For geochemical analysis, twenty-two (22) representative samples of Barail Group from the study area were selected and carried out at the National Geophysical Research

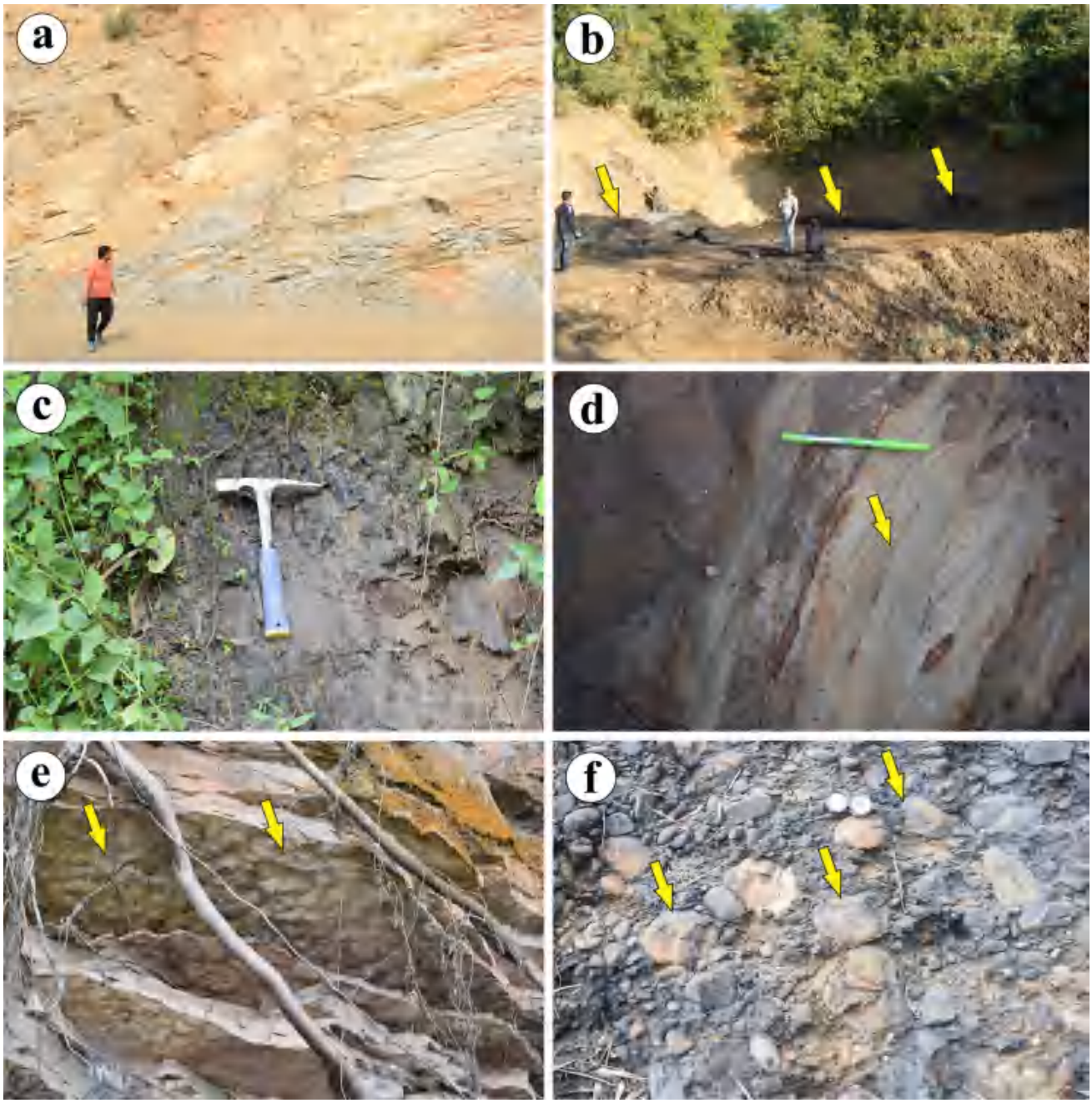

Fig. 2 Field photographs of the study area. **a** Sandstone-dominating Barail Group of rocks, **b** coal seams within the Barail Group (yellow arrow), **c** carbonaceous shale within the Barail Group, **d** cross laminations (yellow arrow), **e** current ripples (yellow arrow), and **f** rounded and elongated pebbles and boulders observed within the Barail Group (yellow arrow)

Institute, Hyderabad, India. Major oxides were examined using XRF, while HR-ICP-MS was employed for the analysis of Trace and REE. Concentrations of major oxides were determined at NGRI, Hyderabad, India using the Philips MagiX PRO PW2440 XRF instrument. Sample pellets were created at NGRI, filled with boric acid, and evenly spread with the sample. These pellets were then pressed using a hydraulic compression machine and analysed for the measurement of major oxides. Loss on ignition (LOI) was calculated by heating 5 g of each sample at 800 °C, recording initial and final weights. For HR-ICP-MS, rock samples underwent dissolution via a wet chemical method. A test portion of each sample, along with an acid mixture (10 mL of 7:3 HF-HNO_3), was placed in Savillex screw top vessels, and internal standards (5 mL of 1 ng/mL 103Rh) were added. After a 48-h hot plate treatment (~ 140 °C),

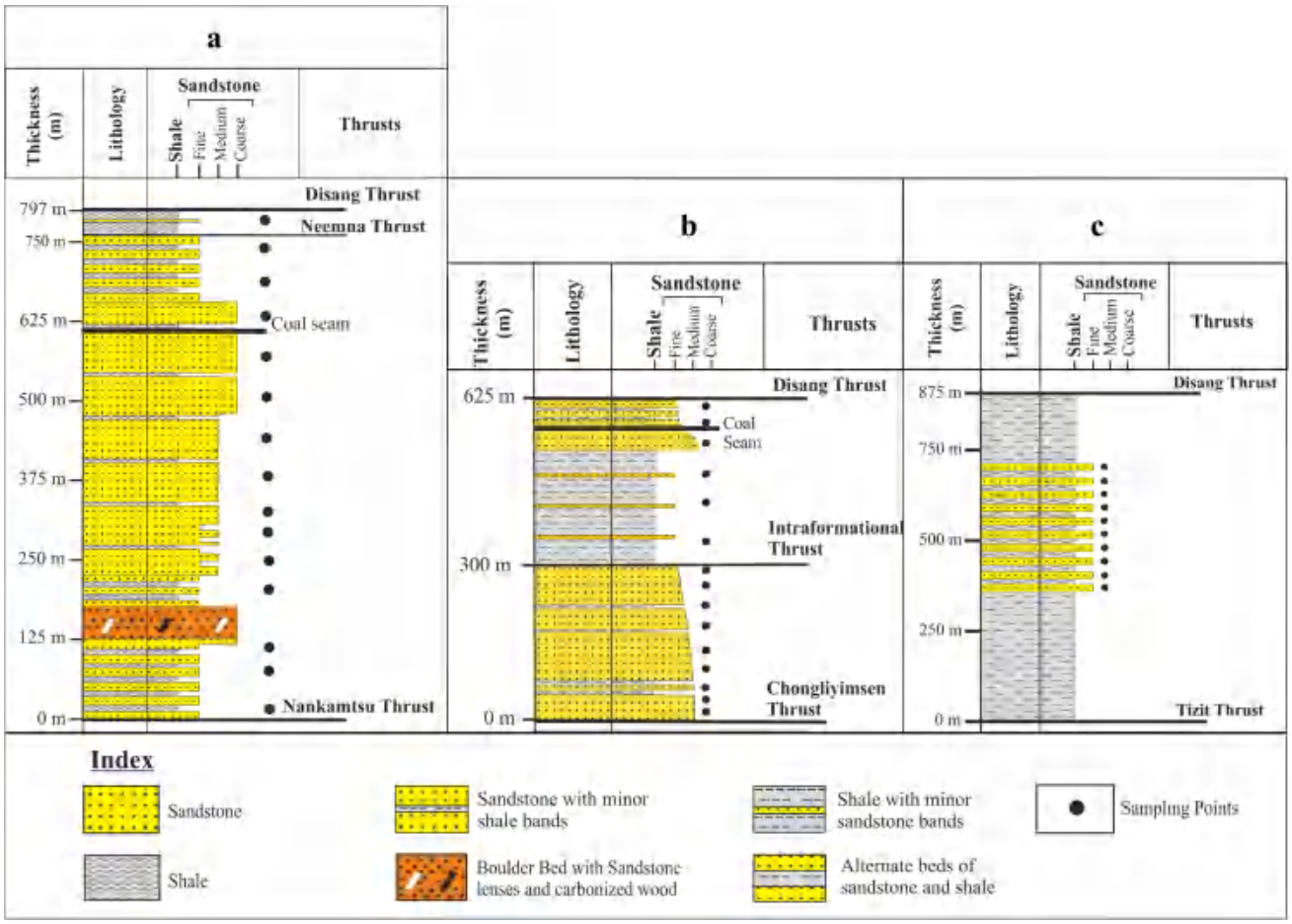

Fig. 3 Litho-column of the Barail Group of rocks of the Belt of Schuppen, Northeast India, along **a** Amguri—Tuli—Merangkong, **b** Mariani—Changki—Longkhim, and **c** Sonari—Tizit—Mon section

samples were evaporated (200 °C) and dissolved, with procedural blanks to account for reagent and handling errors. Selected geological reference samples had certified data for all trace elements. Clear solutions were obtained for all samples, and HR-ICP-MS analysis was conducted using Nu Instruments Attom, UK. Accuracy and precision were determined through replicate analyses of standards and samples, with calibration using the international reference Sandstone sample (GSR-4). The precisions for Major, Trace, and REE analyses were found to be 2% RSD (Relative Standard Deviation), with comparable accuracy, following the methodology of Satyanarayanan et al. 2018.

4 Petrography of the Barail sandstones

4.1 Detrital components

The studied Barail sandstones have quartz as the most dominant mineral in the form of monocrystalline and polycrystalline, and its concentration varies from 42.07% to 62.02 % (avg. 50.39%). Monocrystalline quartz is again recorded as undulose (16.22–21.87 %) and non-undulose (14.32–20.20 %) types, with the former being relatively dominant (Fig. 4a). The polycrystalline quartz is recorded as 2–3 units (2.67–8.89 %) and > 3 units (4.67–12.10 %) per grain. The polycrystalline varieties include recrystallized metamorphic quartz (Fig. 4b) and sheared or stretched metamorphic quartz. Quartz overgrowths are seen in some sandstone (Fig. 4c). The feldspar concentration varies between 0.00% to 2.79% (avg. 1.19%) and is represented by plagioclase (Fig. 4d) and microcline. Mica varies from 1.2 % to 7.77 % (avg. 4.28 %), among which muscovite (Fig. 4e) is more common with minor fractions of biotite. The percentage of rock fragments varies from 5.46 % to 16.93 % (avg. 12.39 %). Sedimentary rock fragments are recorded mainly as weathered shale (Fig. 4f) and siltstones. Metamorphic rock fragments are identified as schistose and gneissic fragments (Fig. 4g). Most of the grains are cemented by silica (Fig. 4h). Ferruginous cement is also common (Fig. 4i).

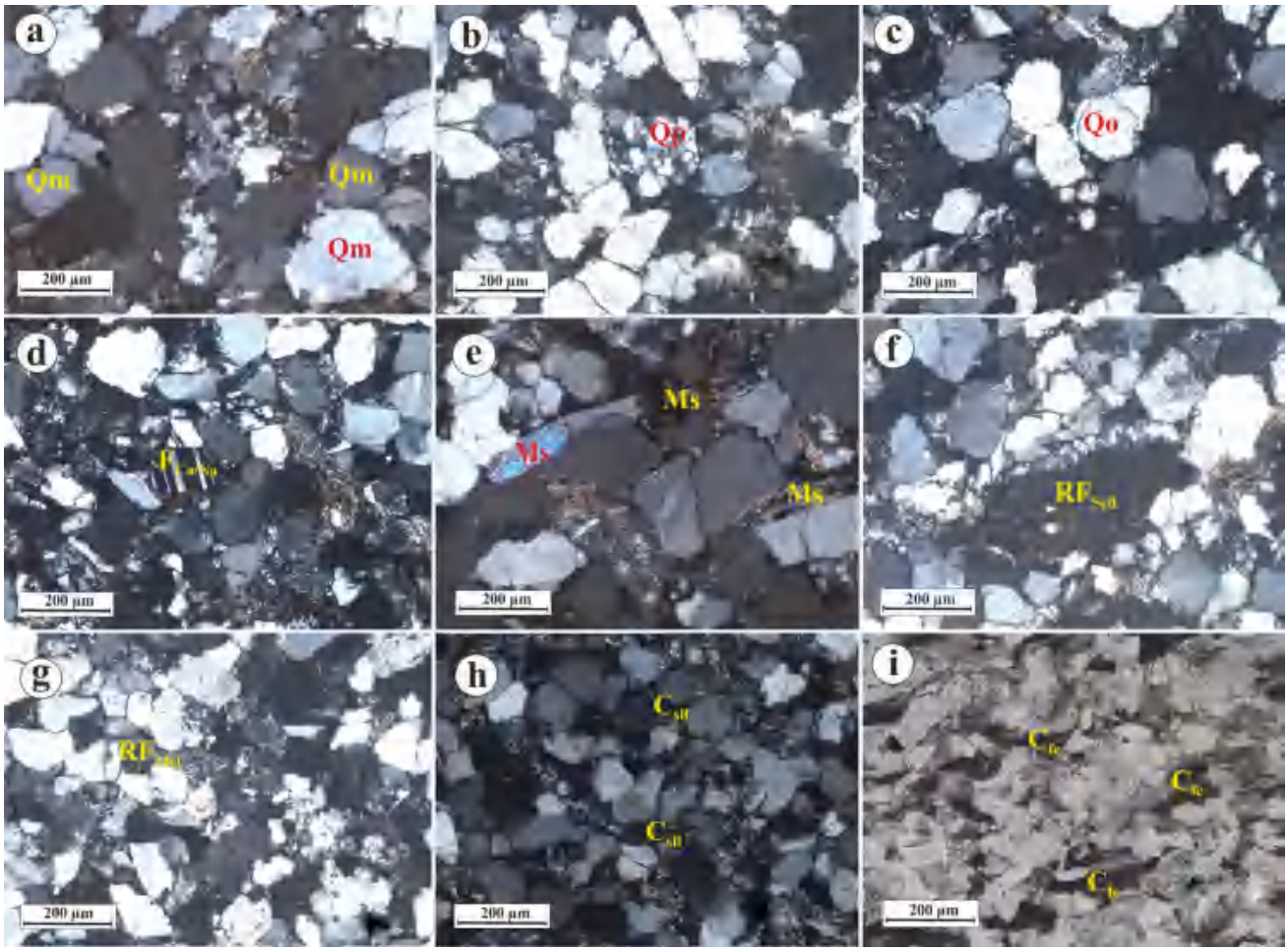

Fig. 4 Photomicrographs of the Barail sandstones. **a** Monocrystalline quartz (Qm), **b** polycrystalline quartz (Qp), **c** quartz overgrowth (Qo), **d** plagioclase feldspar ($F_{Ca/Na}$), **e** muscovite (Ms), **b** sedimentary rock fragment (RF_{sed}), **g** metamorphic rock fragment (RF_{Met}), **h** siliceous cement (C_{sil}), and **i** ferruginous cement (C_{fe})

Cementing material ranges between 12.22 % to 22.34 % by volume. The matrix content in the Barail sandstone varies between 6.44 % to 20.02 %. The modal analysis data of the studied sandstones of the Barail Group is presented in Table S2.

4.2 Diagenesis

The diagenetic effects observed in the Barail sandstones of the present study are cementation, compaction, grain deformation and fracturing, dissolution and replacement, recrystallization, and authigenesis.

4.3 Cementation

The cement types identified in the studied sandstones are silica cement, iron cement, clay cement, and calcareous cement. The silica cement is dominant over the other types of cement present in the rock. It occurs as euhedral syntaxial overgrowths around detrital quartz grains (Fig. 5a). The carbonate cement tends to corrode the grain margins and produce irregularly shaped grains within the sandstones of the Barail Group (Fig. 5b). Iron oxide as reddish-brown cement occurs as pore-filling cement, with thin coatings around detrital grains of the Barail Group (Fig. 5c).

4.4 Compaction

In the studied sandstone, the degree of compaction varies considerably. In the case of more rigid grains, the physical compaction caused floating and point contacts to become long contacts (Fig. 5d) and fracturing of rigid framework components within the sandstones (Fig. 5e). After the burial, the ductile grains had undergone squeezing effects between quartz grains as compaction continued, forming dispersed pseudo-matrix (Fig. 5f). Stylolites are also formed due to the intrastratal solution effect circulating under pressure (Fig. 6a).

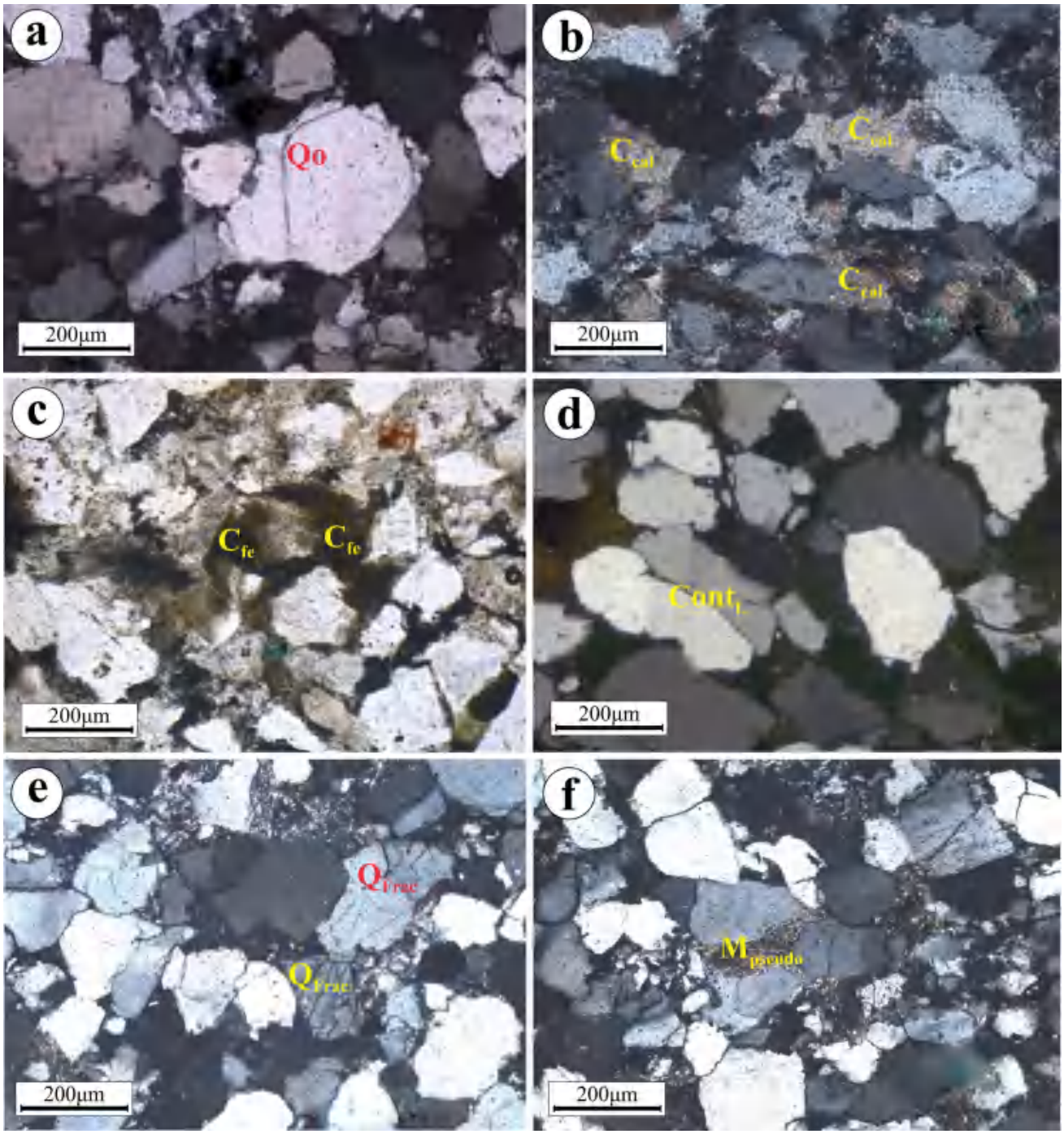

Fig. 5 Photomicrographs of the Barail sandstones. **a** Quartz overgrowths (Qo), **b** carbonate cement tends to corrode the grain margins (C_{cal}), **c** iron oxide occurs as pore-filling cement (C_{fe}), **d** physical compaction causes floating and point contacts to become long contacts ($Cont_L$), **e** fracturing of rigid framework components (Q_{Frac}), and **f** pseudo-matrix (M_{pseudo})

4.5 Grain deformation and fracturing

Grain fracturing, though not intense, is observed on some detrital quartz grains of the studied sandstone. Within certain sandstones of the Barail Group, some mica flakes show compaction effects, as they exhibit microfractures and kink bend with jagged corners around detrital grains (Fig. 6b).

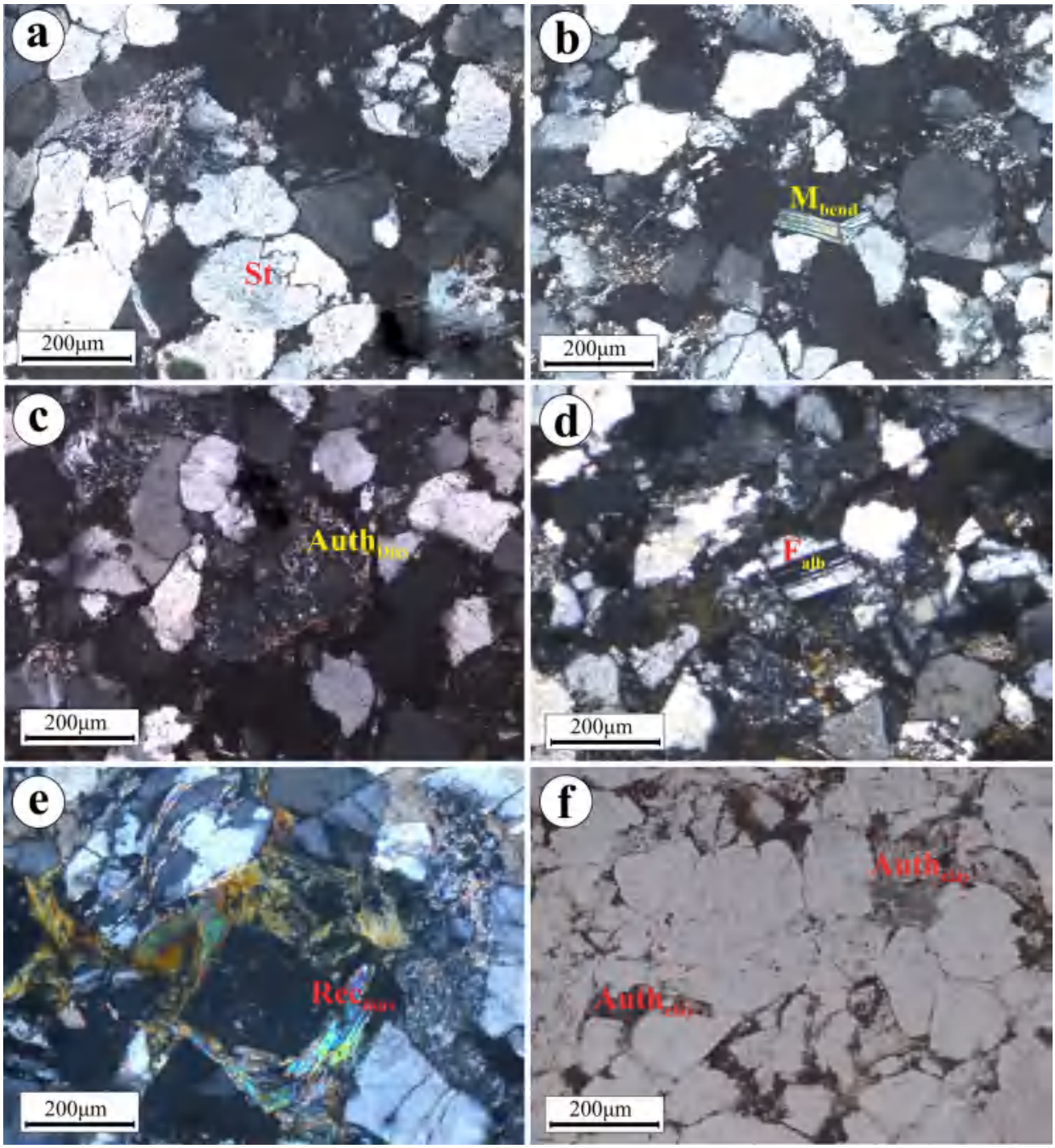

Fig. 6 Photomicrographs of the Barail sandstones. **a** Stylolites formed due to the intrastratal solution effect (St), **b** kink bend of mica flake showing compaction effects (M_{bend}), **c** dissolution of the authigenic minerals ($Auth_{Diss}$), **d** albitized feldspars (F_{alb}), **e** recrystallization of clay minerals to muscovite (Rec_{mus}), and **f** authigenic clay minerals are occurring as pore-filling and pore-lining ($Auth_{clay}$)

4.6 Dissolution and replacement

Secondary porosity has been created by the dissolution of the authigenic minerals or sedimentary grains within the Barail sandstones (Fig. 6c). Albitization of feldspar involves the replacement of weak detrital K-feldspar to albite and promotes secondary porosity. Under the thin sections, albitized feldspars (Fig. 6d) show indistinct and diffused twinning with a cloudy appearance.

4.7 Recrystallization and authigenesis

Recrystallization of clay minerals to muscovite (Fig. 6e) under deep burial compaction indicates late diagenesis found within the Barail sandstones. Such recrystallization increases grain size and negatively affects porosity and permeability (Borgohain et al. 2021). Authigenic clay minerals occur as pore-filling and pore-lining in the studied sandstones (Fig. 6f).

5 Geochemical characteristics of the Barail sandstones

5.1 Major oxides

Major oxide composition in terms of the weight percentage of the Barail sandstones is shown in Table S3. The Barail sandstones are characterized with the high concentration of SiO_2 (54.82–81.00 wt %, avg. 66.19 wt%) followed by lower content of Al_2O_3 (11.38–29.06 wt%, avg. 18.71 wt%), Fe_2O_3 (0.74–16.24 wt%, avg. 5.37 wt%), MgO (0.51–7.51 wt%, avg. 1.98 wt%), K_2O (0.70–3.18 wt%, avg. 1.94 wt%), TiO_2 (0.78–2.45 wt%, avg. 1.28 wt%), Na_2O (0.33–2.12 wt%, avg. 0.97 wt%), CaO (BDL–2.03 wt%, avg. 0.60 wt%), MnO (0.02–0.64 wt%, avg. 0.19 wt%), and P_2O_5 (BDL–0.26 wt%, avg. 0.08 wt%) (Table S3). High to moderate SiO_2 and Al_2O_3 concentration with low Fe_2O_3, MgO, Na_2O resembles the composition of Upper Continental Crust (UCC). The concentrations of SiO_2 show negative correlations with Al_2O_3 ($r = -0.28$), Fe_2O_3 ($r = -0.66$), MnO ($r = -0.04$), MgO ($r = -0.29$), CaO ($r = -0.35$), Na_2O ($r = -0.21$), K_2O ($r = -0.64$) and P_2O_5 ($r = -0.39$), except TiO_2 ($r = 0.17$) showing weak positive correlation (Fig. 7). However, a positive correlation of Al_2O_3 with TiO_2 ($r = 0.43$), MnO ($r = 0.16$), and K_2O ($r = 0.48$) implies the presence of these elements with the rock fragments and with the clay minerals. Fe_2O_3 with MgO ($r = 0.14$), CaO ($r = 0.65$), Na_2O ($r = 0.17$) and P_2O_5 ($r = 0.63$) are also positively correlated (Fig. 8).

The high SiO_2/Al_2O_3 (avg. 3.76 wt%) ratio indicates the influence of recycling processes, weathering, and sediment transport. The Al_2O_3/TiO_2 ratio is also high (avg. 14.94) due to the probable continental derivation of the sediments (Fyffe and Pickerill 1993). The UCC (Taylor and McLennan 1985) normalized (Fig. 9a) pattern of oxides of the samples shows a remarkable depletion of CaO.

5.2 Trace elements

Trace element concentrations of the Barail sandstones are shown in Table S4. Among the various trace elements, Large Ion Lithophile Elements (LILE) are enriched (avg. Rb: 95.59 ppm, Sr: 105.52 ppm, Ba: 297.98 ppm), and High Field Strength Elements (HFSE) are depleted (avg. Th: 15.02 ppm, U: 2.51 ppm, Hf: 6.74 ppm), except Zr (avg. 270.29 ppm) (Table S4). Transitional elements (Sc, Co, Ni) are also depleted (avg. Sc = 15.77 ppm, Co = 14.4 ppm, Ni = 54.31 ppm,), except Cu (avg. 69.45 ppm), Zn (avg. 89.15 ppm), V (avg. 125.31 ppm) and Cr (avg. 143.21 ppm) as compared to the UCC (Taylor and McLennan 1985). Due to detrital interaction with Zircons, Zr has a high concentration (avg. 270.29 ppm). Upper Continental Crust (UCC) normalized values of all the trace elements are plotted as shown in Fig. 9b (Taylor and McLennan 1985). The plot shows the depletion of elements like Sr (avg. 0.33), Ba (avg. 0.47), and Co (avg. 0.82) in comparison to UCC (Taylor and McLennan 1985).

5.3 Rare earth elements (REE)

The concentration of REE, along with certain elemental ratios of Barail sandstones, is represented in Table S4. The Chondrite normalized patterns of REE concentration are shown in Fig. 9c, which shows the Light Rare Earth Elements (LREE: La-Gd) are enriched over Heavy Rare Earth Elements (HREE: Tb-Lu), with LREE/HREE ratio is 5.77 to 13.61 (avg. 8.98 ppm). Barail sediments showed a negative Eu anomaly (i.e., $Eu/Eu^* < 1$) with an average of 0.66 (Table S4). The $(La/Yb)_N$ ratio ranged from 6.67–20 with an average of 11.14, comparatively higher than UCC: 10.47 (Taylor and McLennan 1985). The Chondrite normalized $(La/Sm)_N = 3.15–4.63$ (avg. of 3.59) and $(Gd/Yb)_N = 1.21$ to 2.92 (avg. 1.93) ratio bears a resemblance with the UCC (Taylor and McLennan 1985).

6 Discussion

6.1 Texture and sandstone classification

The petrographic data shows that the sandstones have a higher concentration of quartz and a relatively smaller proportion of rock fragments, feldspar, and mica. Grains are moderate to ill-sorted and sub-angular to sub-rounded in shape. Sandstones having a higher percentage of matrix show less cement content. The sandstone classification after Folk (1980) shows that the Barail sandstones are sublithic arenite type (Fig. 10a). Again, following the classification proposed by Pettijohn (1972), it is seen that the studied sandstones are mostly sublithic arenite to lithic greywacke varieties (Fig. 10b).

Major elemental concentrations are utilized to classify sandstones (Pettijohn et al. 1972; Blatt et al. 1980). In the classification scheme after Pettijohn et al. (1972), the logarithmic values of the ratio of (SiO_2/Al_2O_3) *vs.* (Na_2O/K_2O) are used, where most of the samples are clustered as

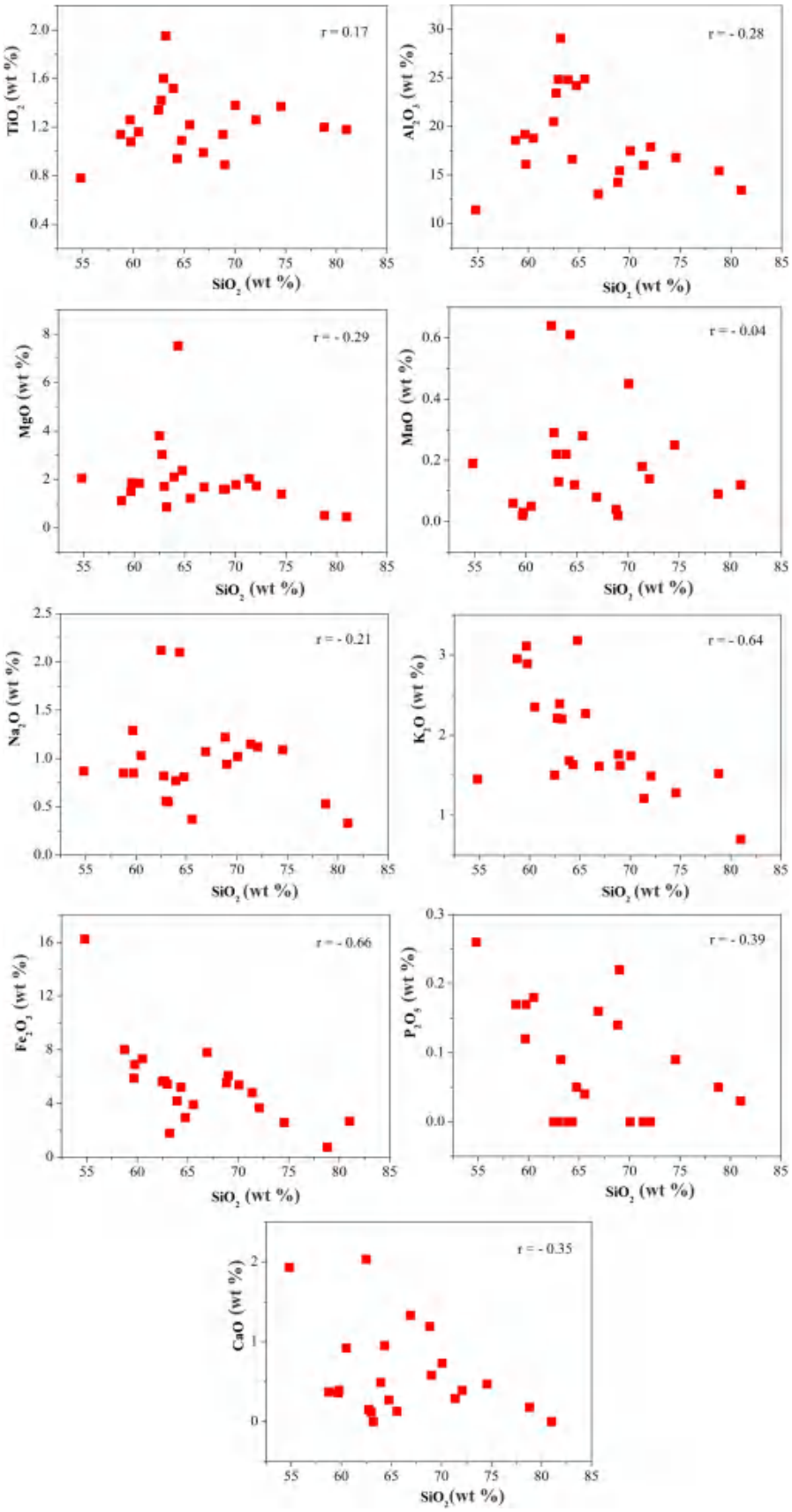

Fig. 7 Variation diagram for correlation between wt% of SiO_2 vs. major oxides

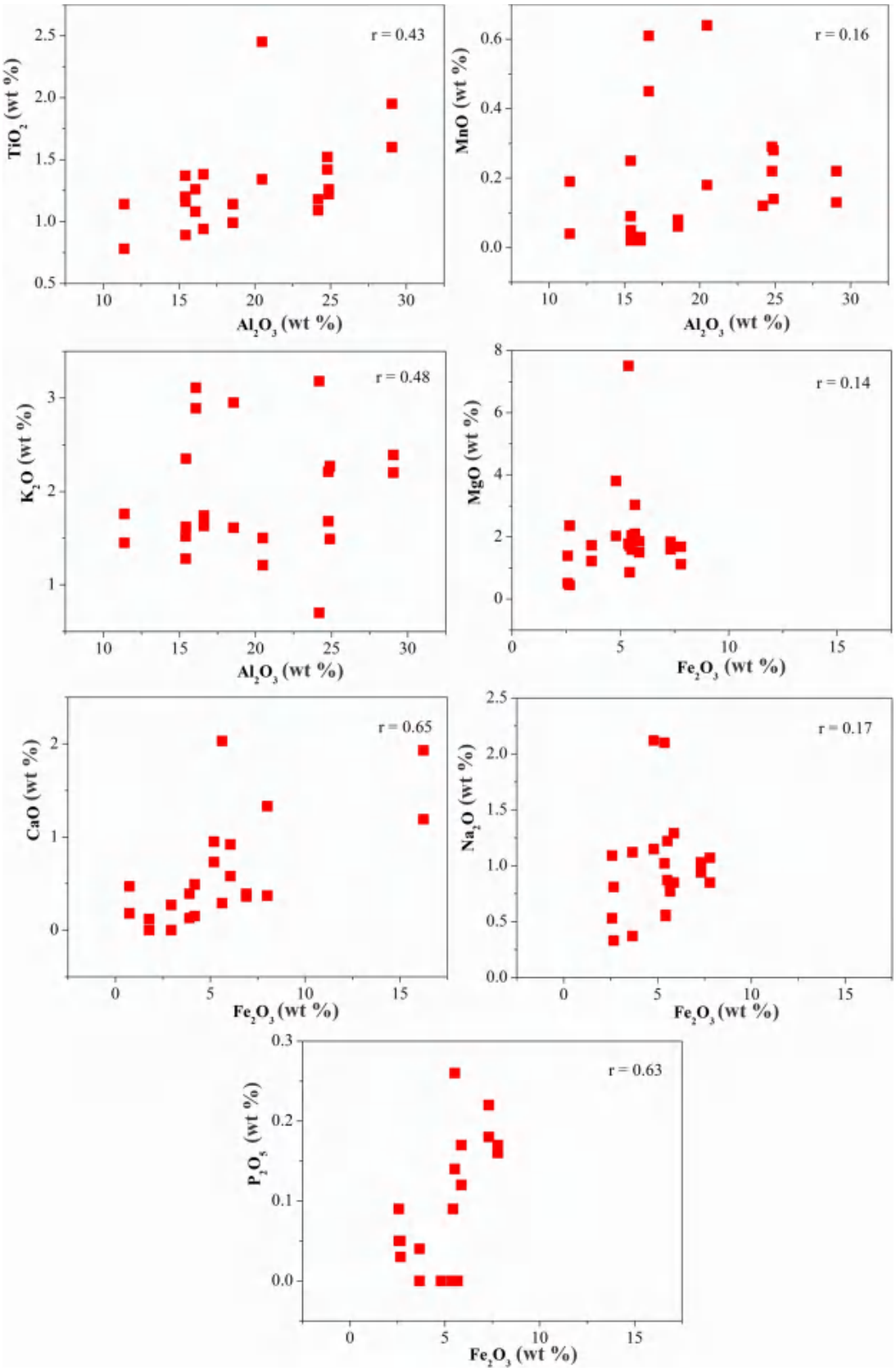

Fig. 8 Variation diagram for correlation between wt% of major oxides

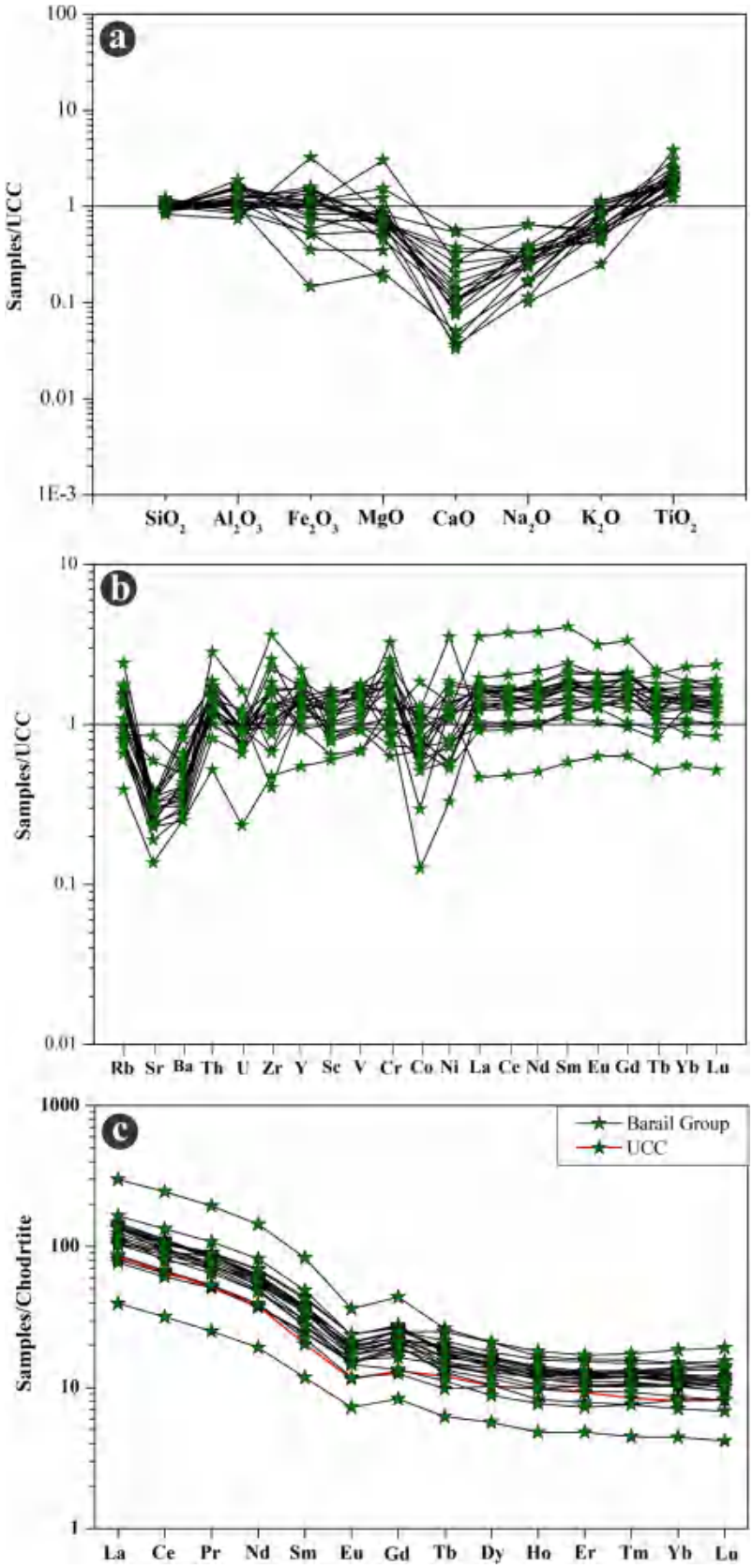

Fig. 9 **a** UCC normalized plot for major oxides, **b** UCC normalized multi-element plot, and **c** chondrite normalised REE patterns (Tailor and McLennan 1985) of the Barail Group of sediments

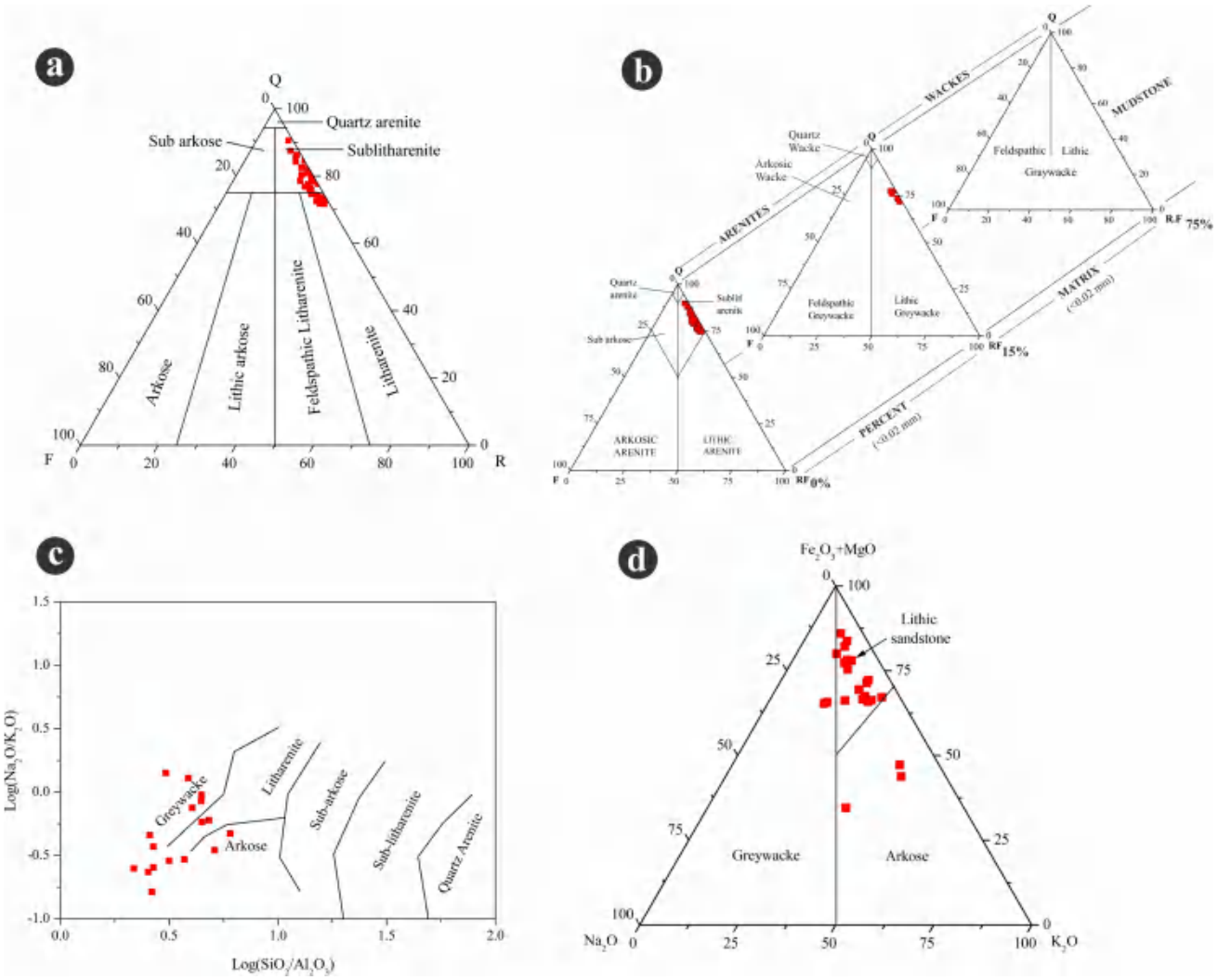

Fig. 10 **a** Classification of sandstones after Folk (1980), **b** petrographical classification after Pettijohn (1972), **c** geochemical classification after Pettijohn et al. (1972), and **d** sandstone classification after Blatt et al. (1980)

litharenite type (Fig. 10c). However, few samples appear to be of arkose and greywacke type. The ternary plot (after Blatt et al. 1980) between wt % values of Na_2O, $Fe_2O_3 + MgO$, and K_2O to classify sandstone types shows that the sandstones are of lithic variety (Fig. 10d).

6.2 Provenance

The nature of the provenance, from where the sediments are derived, may be revealed by the quantitative analysis of different types of terrigenous sediments present in the rock. Basu et al. (1975) and Tortosa et al. (1991) discussed in detail about quartz grains as an indicator of provenance. From the present study, the overall dominance of monocrystalline quartz (avg. 19.45%) over polycrystalline quartz (avg. 13.91%) indicates the sediments are primarily derived from the metamorphic sources (Blatt et al. 1980). The dominance of polycrystalline quartz in the studied sandstones suggests their derivation of sediments from low-grade metamorphic rocks (Basu et al. 1975), which is also observed in the diamond diagram plot of Basu et al. (1975), as shown in Fig. 11a. Quartz grains with undulatory extinction are weak because they have been plastically deformed (Folk 1980). The enrichment of undulose and non-undulose monocrystalline quartz over polycrystalline quartz in the studied sandstones suggests plutonic and low-rank metamorphic sources (Folk 1980). The diamond plot after Tortosa et al. (1991) also indicates the derivation of Barail sediments from granite and gneisses (Fig. 11b). Both sedimentary and metamorphic lithic fragments indicate the derivation of sediments from sedimentary and metamorphic terrain. The presence of detrital chert corroborates a sedimentary source of the Barail Group of sediments.

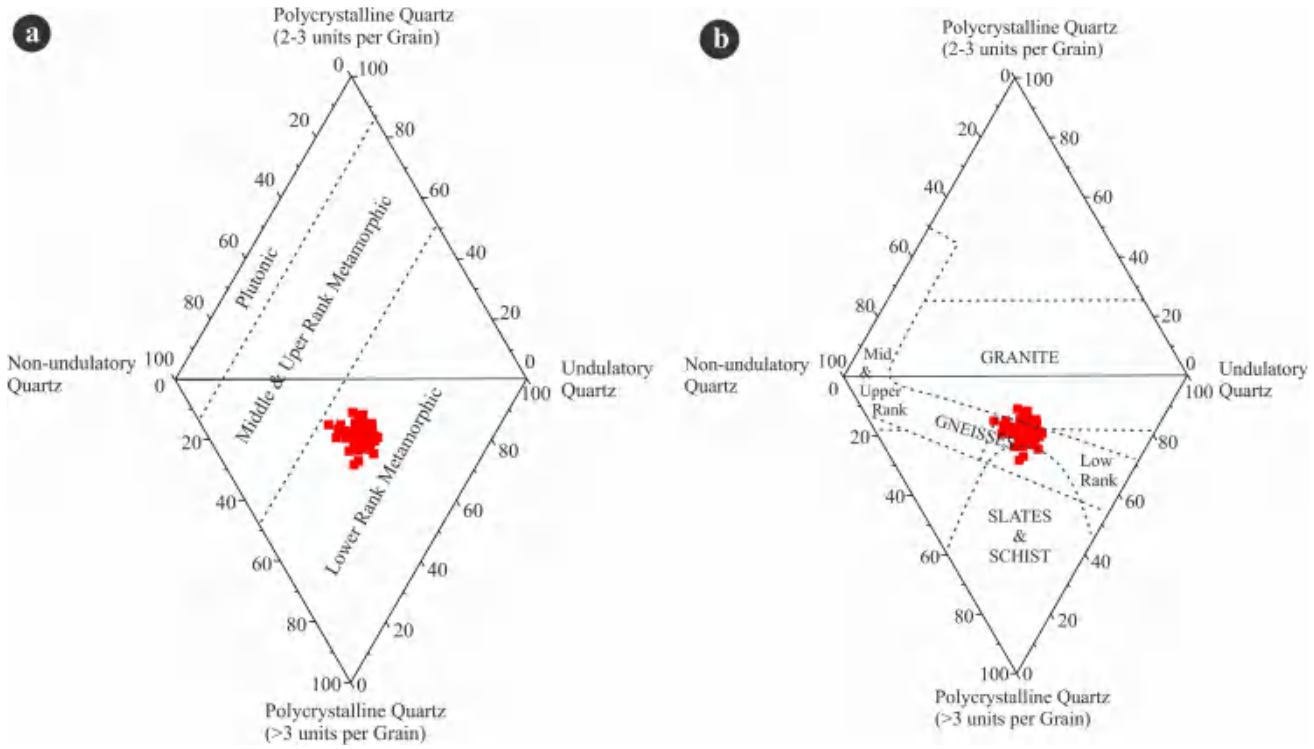

Fig. 11 **a** Diamond plot for provenance after Basu et al. (1975) representing their derivation of sediments of the Barail Group from low-rank metamorphic, and **b** diamond plot for provenance after Tortosa et al. (1991) representing their derivation of sediments of the Barail Group from granite and gneisses

6.3 Geochemical characteristics of the provenance

Trace and REE Geochemistry is a replica of source rocks for clastic sedimentary rocks. Hence the concentration of source rocks could be used in sediment geochemistry to correlate with the geochemical signature of the sediments. Because of their immobile and limited fractionation behavior trace and REE elemental concentration are used as bivariate and ternary plot to understand the nature and characteristics of source rocks (Taylor and McLennan 1985; Bhatia and Crook 1986; McLennan and Hanson 1993). To understand the nature of source rocks and their possible origin we are using various ternary and bivarite plot of intermixing of different source rock plots (La–Th–Sc after Jinliang and Xin 2008; Sc vs Th/Sc after Schoenborn and Fedo 2011; Y/Ni vs Cr/V after Mongelli et al. 2006; Th × 10-V-Ni after Bracciali et al. 2007; Zr/Sc vs Th/Sc after McLennan and Hanson 1993 and few bivariate plots by using certain trace and REE ratios).

Ternary plot of La-Th-Sc by Jinliang and Xin (2008) is a representation source rock intermixing of Granite (with Eu/Eu*: 0.5 and Th/Sc: 1.18) and Granodiorite (with Eu/Eu*: 0.7 and Th/Sc: 0.5). Barail sediments are indicative of possible derivation primarily from granitic sources as supported by the average ratio of Eu/Eu*: 0.68 and Th/Sc: 0.99 as well as significant contribution from granodiorite as shown in Fig. 12a. Again the bivariate plot of Sc vs Th/Sc by Schoenborn and Fedo (2011) is a quantitative estimation for intermixing of different source rocks. Barail sediments are with average ratio of Th/Sc = 0.99 which resembles the mixing model Th/Sc ratio (1.15). In Fig. 12b Barail sandstones are clustered near 90% Granodiorite + 10% high K-Granite field which is indicative of the contribution of the sediments primarily from intermixing of granodiorite and granitic sources. A similar observation has resulted from the bivariate plot of ganitic indicator: Y/Ni vs ultramafic indicator: Cr/V (Mongelli et al. 2006) where the Barail sandstones are scattered near the granitic field (Fig. 12c). Moreover, the ternary plot of Th × 10-V-Ni (Bracciali et al. 2007) representing a possible derivation of felsic rocks rather than the mafic and ultramafics (Fig. 12d). McLennan and Hanson (1993) proposed a bivariate plot by using the Zr/Sc vs Th/Sc which portrays two patterns regarding the source composition and effects on source by recycling processes. In Fig. 12e, majority of the samples are representative of original source rock composition but only a few are following the diverted trend due to possible enrichment of Zircons (avg. Zr: 270 ppm, range: 78–694 ppm) as a result of recycling of sediments before that deposited in the basinal part from the study area. The elemental ratios of trace and rare earth elements have been proposed by Cullers (1994, 2000) and Cullers &

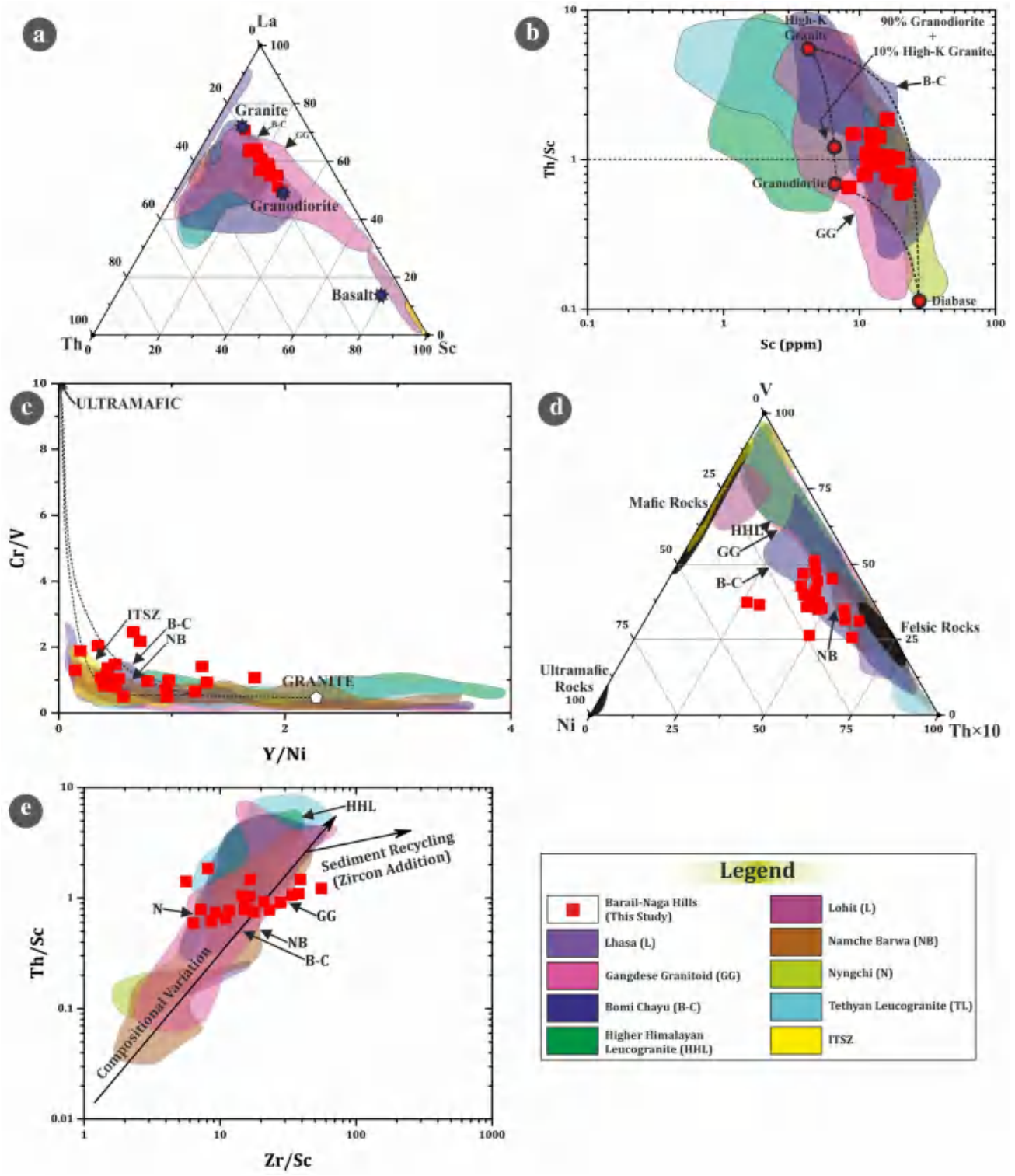

Fig. 12 Provenance plots: **a** ternary plot of La-Th-Sc after Jinliang and Xin (2008); **b** bivariate plot of Sc vs Th/Sc after Schoenborn and Fedo (2011); **c** bivariate plot of Y/Ni vs Cr/V after Mongelli et al. (2006); **d** ternary plot of Th × 10-V-Ni after Bracciali et al. (2007) & **e** bivariate plot of Zr/Sc vs Th/Sc after McLennan and Hanson (1993) representing the source of Barail Group of sediments

Podkovyrov (2002) against different sources as presented in Table S5. The range of the elemental ratios shown by Barail sandstones are: Eu/Eu*: 0.57–0.72, La/Sc: 1.58–6.87, Th/Sc: 0.59–1.58, La/Co: 1.47–18.07, Th/Co: 0.48–6.13, Cr/Th: 5.76–22.66 and La/Lu: 6.63–21.11 indicates the sediments are contributed from felsic source rocks. Similarly, Chondrite-normalized REE pattern (Fig. 9c) and Eu anomaly gives clues about the nature of source rocks (Basu et al. 1975; Armstrong-Altrin 2009). Barail sandstones are showing a fractionated trend [$(La/Lu)_N$: 11.58] and a visible sharp negative Europium anomaly that suggest a fractionated granitic source rock. Based on these geochemical observations it can be mentioned that during Oligocene time sediments have been contributed from tectonic domains that contained primarily of felsic or their metamorphic equivalent source rocks.

6.4 Inference for the source areas

Study area is located south to the eastern Himalayan ranges and adjacent to the Eastern Himalayan Syntaxies at the northeastern corner of India. Himalayan arc system was resulted by the Indian and Eurasian plate collision which occurred during Paleocene-Eocene time ~ 55–51 Ma. (Critelli and Garzanti 1994; Rowley 1996; Pivnik and Wells 1996; Guillot et al. 2003; DeCelles et al. 2004). The Himalayan ranges have been categorized into four tectonic domains that are represented from the north towards the Indian plate as the Tibetan Himalayan Zone (THZ), the Greater Himalayan Zone (GHZ), the Lesser Himalayan Zone (LHZ) and Sub-Himalayan Zone (SHZ). The litho-association of these tectonic domains were basically comprised of granitoids and their various metamorphic equivalents (Reichardt et al. 2010; Ahmad et al. 2008; Zeng et al. 2014; Jiang et al. 2015).

The entire basins of NE India was an open ocean connected to the proto Bengal Basin. Sedimentations occurred mainly from the various tectonic domains which are connected to the basin by the Yarlung-Tsangpo (Paleo-Brahmaputra) formed by the confluence of Siang, Dibang and Lohit river. Studies by Hodges (2000), Liang et al. (2008) and Chiu et al. (2009) have reported that the river Brahmaputra (Yarlung-Tsangpo) was following the marginal zones of Indian-Eurasian plate and continuously draining the Trans-Himalayan Arc, Tethyan Himalayan Zones, Indo Tsangpo Suture Zone (ITSZ) including Indian crust(?). Initially, the river Brahmaputra flowed southerly towards the eastern margin of basins located in NE India (Najman et al. 2016). As the sea beings to recede the delta system prograded in the SSW direction causing enormous deposition of Barail sediments during Oligocene. The Barail sediments deposited along the delta front and delta plain were the regions of formation of sandstones represented by the lithocolumns shown in the Fig. 3. Sedimentation as well as progradation of delta system continued till the end of Miocene (Najman et al. 2016; Clark and Bilham 2008). As a result of upliftment of Shillong Plateau during Middle-Late Miocene time and rise of Naga Hills from Early Miocene (Clark and Bilham, 2008; Morley and Searle, 2017) were the possible cause for the diversion of Paleo-Brahmaputra shifting towards west as it flows at the present day. The shifting of river Brahmaputra and southwestern regression of shoreline is witnessed by the deposition of fluvial Tipam sediments (Late Miocene-Early Pliocene) in different parts of Upper Assam, Naga Hill ranges and Surma Basin. This regression can also be represented in the geological map as represented in the Fig. 1b where younger sediments are exposed towards the eastern margin, as a result of upliftment of Indo-Burmese ranges due to collision between Indian plate with the Burmese micro plate. Moreover, Rao (1983) also reported the existence of lacustrine (Late Pliocene) areas, southeast of the Shillong plateau, that was probably formed due to the upliftment of the easterly located Naga Hills and Surma Basin that also restricting the flow of river Brahmaputra.

To characterize the provenance certain tectonic domains from the THA, THZ including ITSZ are considered for this study that continuously shedding by the Paleo-Brahmaputra. In order to correlate the geochemical signature of these domain with the Barail sediments we have plotted various published data from the Himalayan ranges and Eastern Himalayan syntaxies in different provenance plots as well some of the bivariate plots by using the ratios of trace and REE. Here we are considering the tectonic domains of Himalayan ranges and Eastern Himalayan Syntaxies including: Higher Himalayan Leucogranite (Gao et al. 2019; Huang et al. 2017; Tian et al. 2017; Visonà et al. 2002; Yang et al. 2019; Zhang et al. 2004), Tethyan Leucogranite (Gao et al. 2019; Liu et al. 2014, 2016; Xiao et al. 2008; Zeng et al. 2015), Gangdese Granitoid (Chen et al. 2015, 2019a, 2019b; Guo et al. 2011, 2013; Ma et al. 2017; Meng et al. 2016; Wang et al. 2015, 2016; Xu et al. 2015; Zhang et al. 2010a, 2010b, 2014; Zhou et al. 2017), ITSZ (Bédard et al. 2009; Bezard et al. 2011; Dai et al. 2013; Dubois-Côté et al. 2005; Guilmette et al. 2009; Wang et al. 2018; Zheng et al. 2017; Zhong et al. 2019), Lhasa Terrain (Ding et al. 2003; Harrison et al. 2000; Zhu et al. 2009), Bomi-Chayu (Chen et al. 2019a, b; Dong et al. 2019; Lai & Zhu 2019; Lin et al. 2012; Pan et al. 2012; Xie et al. 2020; Xu et al. 2013; Zhu et al. 2017, 2020), Namche-Barwa (Gao et al. 2019; Ji et al. 2017; Tian et al. 2020; Zhang et al. 2012), Nyngchi (Guo et al. 2019; Zhang et al. 2010a, 2010b, 2013) and Lohit Batholith (Bikramaditya et al. 2020; Haproff et al. 2019) for the purpose of this study. These domains are connected either by Yarlung-Tsangpo (paleo-Brahmaputra) or by their major tributaries. While plotting a large dataset of Himalayan ranges and EHS in various binary and ternary plot in which we are representing each dataset with different fields by using different

colors, the index of which is given in the figure. Figure 12 is a representation of various provenance plots: La–Th–Sc after Jinliang and Xin (2008); Sc vs Th/Sc after Schoenborn and Fedo (2011); Y/Ni vs Cr/V after Mongelli et al. (2006); Th × 10–V–Ni after Bracciali et al. (2007) and Zr/Sc vs Th/Sc after McLennan and Hanson (1993), where it is showing that majority of the Barail sandstone samples are overlapping within the fields of Bomi-Chayu, Gangdese Granitoid and Namche Barwa. Moreover we are preparing some of the bivariate plots (Fig. 13a,b) by using ratios of Trace and REE (Eu/Eu*, Ce/Ce*, Th/U, Zr/Sc, V/Y, LREE/HREE, La/Lu, La/Nd, Zr/Zn, La/Sm, La/Th and V/Ni) which mainly bears the geochemical signature of provenance. These ratios can be used for targeting the provenance and they better represents the provenance rather than using the individual concentration of some specific element. In this figure, we also make fields of different domains by using some specific colors and in the same diagram we have plotted the Barail sandstone samples for the correlation purpose. The domains which are highlighted with arrow mark are showing almost similar geochemical behavior with the studied sediment samples. The summary of which is given in the Table S6 that represents 3 major domains that contributed the majority of the sediments. We observed for the Figs. 12 & 13 that the majority of the sediments have been contributed from the Bomi-Chayu, Gangdese Granitoid, Higher Himalayan Leucogranite and Namche Barwa with some minor contributions from ITSZ and Tethyan Leucogranite. Moreover, we also plotted certain standards viz. Granite, Basalt, Andesite, Tonalite–Trondhjemite–Granodiorite, Felsic Volcanics, Sandstone (avg. of all time), Cratonic Sandstone, Cratonic Shale and Upper Continental Crust, all values are proposed by Condie 1993. While correlating with these standards we observed that our studied samples are geochemically similar to Tonalite–Trondhjemite–Granodiorite, Felsic Volcanics, Andesite etc. which geochemically represents sedimentation from arc-derived source rocks that actually infers subduction tectonics like Himalayan arc. Barail sandstones are also geochemically similar to Cratonic Shale, Cratonic Sandstone and Sandstone as well as they are identical to the standard UCC. Therefore we can infer that in the basinal part of the study area sediments are contributed from these domains by the Paleo-Brahmaputra (Yarlung-Tsangpo) and some antecedent rivers that do not have their existence at the present day. This also indicates the geochemical signature of various source rocks from these domains and the studied Barail sediments are similar, as we know that their concentration/ratios are not been modified by the sedimentation processes.

6.5 Tectonic setting

Dickinson and Suczek (1979) documented that sandstone composition derived from different kinds of provenance terrains controlled by plate tectonics. According to Dickinson and Suczek (1979), plate tectonics controls sandstone compositions produced from various terrains. The recalculated point-counting data of rock thin sections (Table S2) of the studied sandstones are plotted in Q-F-L (after Dickinson and Suczek 1979) and Q_m-F-L_t (after Dickinson et al. 1983) diagrams following. From the Q-F-L (Fig. 14a) and Q_m-F-L_t (Fig. 14b) plots, it appears that the Barail sediments are the products of the recycled orogen. The sediments are derived from sedimentary and metamorphic rocks exposed to erosion by the orogenic uplift of fold-thrust belts in recycled orogens (Dickinson and Suczek 1979, Dickinson 1983).

The chemical composition of the clastic sedimentary rocks is dependent mainly upon the source area characteristics and their geological setting (Bhatia 1983; Bhatia and Crook 1986). Several approaches based on the geochemical composition of clastic sediments have been proposed to decipher the tectonic setting throughout the last few decades. In the present study, a few commonly used plottings of Roser and Krosch (1986), Bhatia (1983), Bhatia and Crook (1986) are used to evaluate the tectonic setting. In the binary plot of SiO_2 vs. K_2O/Na_2O (after Roser and Krosch 1986), as represented in Fig. 15a, most of the studied samples show clustering in the active continental margin setup. Moreover, the binary discrimination plot (after Bhatia 1983) of the studied Barail Group of samples depicts the active continental margin setup (Fig. 15b). However, the trace element-based ternary diagram, i.e., Th–Sc–Zr/10 (after Bhatia and Crook 1986), shows the Barail Group of sediment clustering mainly in the continental island arc setting (Fig. 15c).

6.6 Paleo-climate & Paleo-weathering

Climate change is a significant factor in altering the composition of sediments and their population. According to Suttner et al. (1981), the large population of quartz and relatively lower proportion of feldspar and rock fragments in the studied sandstones indicate that the sediments were derived under humid climatic conditions. The average relative percentages of quartz, feldspar and rock fragments of the Barail sandstones are 81.82%, 1.9%, and 16.28%, respectively. The QFR ternary plot proposed by Suttner et al. (1981) is helpful in deciphering the paleoclimatic condition. The plot shows the clustering of the Barail Group of sandstones in the metamorphic (humid) field (Fig. 16a). Moreover, the weathering index: $WI = C \times R$ (WI-Weathering index, C-Climate, and R-Relief) (after Grantham and Velbel 1988) and the bivariate plot of ln(Q/R) vs. ln(Q/F) (after Weltje 1994) also indicate the similar nature of the paleoclimate (Fig. 16b). It is observed that sediments of the Barail Group represent metamorphic sources with weathering indices between 1–2, suggesting humid to sub-humid paleoclimatic conditions and moderate weathering. The bivariate plot of ratios

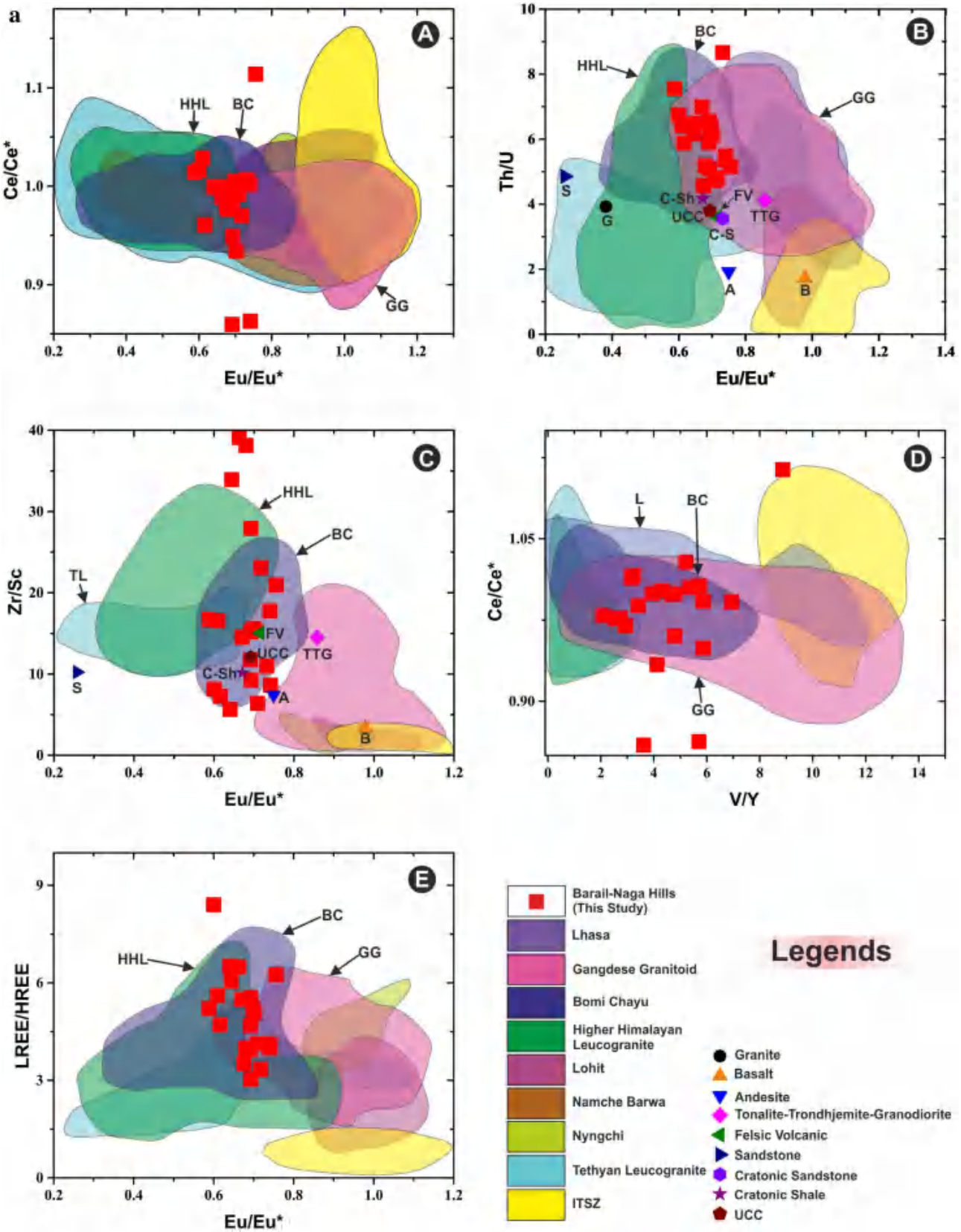

Fig. 13 Bivariate plot of Eu/Eu* vs Ce/Ce*, Eu/Eu* vs Th/U, Eu/Eu* vs Zr/Sc, V/Y vs Ce/Ce*, Eu/Eu* vs LREE/HREE, La/Lu vs Eu/Eu*, La/Nd vs Zr/Zn, La/Sm vs Ce/Ce*, La/Th vs Ce/Ce*, Th/U vs La/Lu and V/Ni vs Ce/Ce* representing the tectonic domains contributed a majority of the sediments to the basin (HHL: Higher Himalayan Leucogranite; BC: Bomi-Chayu; GG: Gangdese Granitoid; TL: Tethyan Leucogranite; L: Lohit; N: Nyngchi & ITSZ: Indus-Tsangpo Suture Zone)

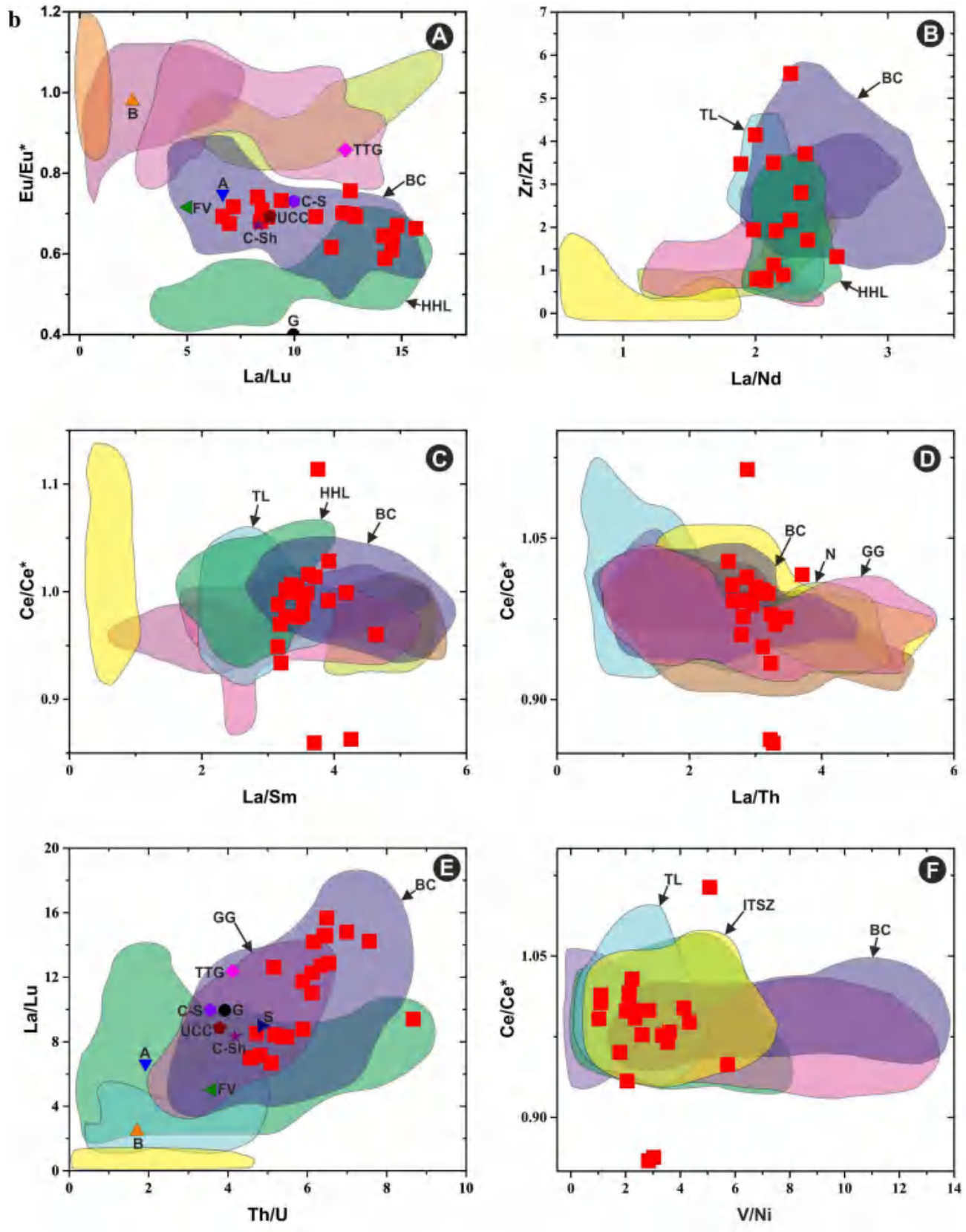

Fig. 13 (continued)

of (Q_{Total}/F + RF) vs. (Q_P/F + RF) (after Suttner and Dutta 1986) also supports the above observations of climatic conditions where samples are clustered in humid to semi-humid climatic conditions (Fig. 16c). The geochemical signature of sediments in terms of distribution and concentration of certain major and trace elements provides vital information regarding the paleoclimate and paleoenvironmental conditions during the sedimentation processes (Getaneh 2002; Moradi et al. 2016). Based on elemental concentration of sediments, Zhao et al. (2007), Cao et al. (2012) and Moradi et al. 2016 proposed the C-Value as an indicator of paleoclimate, which defines as C-Value = ∑(Fe + Mn + Cr + Ni + V + Co)/∑(Ca + Mg + Sr + Ba + K + Na). C-Value provides important clues about the changes in paleoclimatic conditions from warm and humid to hot and arid primarily based on the generally accepted hypotheses suggesting that Fe, Mn, Cr, Ni, V, and Co are relatively enriched under moist conditions, whereas Ca, Mg, Sr, Ba, K, and Na are concentrated under arid conditions due to the precipitation of saline minerals as a result of evaporation (Zhao et al. 2007; Cao et al. 2012). The C-Value of clastic sediments has been widely used as a powerful tool to represent the paleoclimate in the last decade (Moradi et al. 2016; Tao et al. 2017; Fathy et al. 2018; Li et al. 2019; Zhao et al. 2021; Wu et al. 2022; Ma et al. 2023). A modified version of C-Value known as Palaeoclimatic Factor (PF) is proposed by Samad et al. (2020) with the incorporation of Rb and Ti instead of Mn, Cr and Co: PF = ∑(Fe + V + Ni + Rb + Ti)/∑(Ca + Mg + Sr + Ba + K + Na). While calculating the C-Value for Barail sediments showing a range of 0.28—2.57 with an average of 1.01. Palaeoclimatic Factor (PF) is also showing similar with the C-Value, for Barails the range is 0.52—2.64 with an average of 1.20. This indicates during the sedimentation of Barail Group of rocks, the prevailing paleoclimatic condition was under warm and sub-humid to humid conditions. This observation is also substantiated by the Sr/Cu (Lerman and Gat 1989) and Rb/Sr (Jin and Zhang 2002; Bai et al. 2015) ratios which are considered as paleoclimatic indicators. Barail sediments are showing a range of Sr/Cu: 0.35—4.65 with an average of 2.04 indicating warm and humid climatic condition (> 5 for hot arid, 1.3—5.0 for warm and humid) prevailing at the time of sedimentation. Similarly, Rb/Sr ratio of Barails are: 0.26–1.80 (avg. 0.97) indicating a moderate value representing a humid and warm condition during the sedimentation (high ratios for cold while low ratios reflect warm conditions). Hence both Sr/Cu and Rb/Sr ratios strongly support the C-Value and PF as well as the petrographical bivariate plots that during the deposition of Barails the sedimentation occurred under warm and sub-humid to humid climatic conditions.

The change in the mineralogical and chemical composition of clastic rocks is influenced by chemical weathering in the source area (Nesbitt et al. 1996). Several geochemical weathering indices have been proposed in recent decades, including the Chemical Index of Alteration (CIA) (after Nesbitt and Young 1982), Chemical Index of Weathering (CIW) (after Harnois 1988), Weathering Index of Parker (WIP) (after Parker 1970), Plagioclase Index of Alteration (PIA) (after Fedo et al. 1995), and Index of Chemical Variability (ICV) (after Cox et al. 1995) are widely used to deduce the paleoclimatic conditions of clastic sedimentary rocks, including the extent to which the source rocks have been weathered by using the major element concentrations. The mathematical derivations of these parameters are given below: (where, CaO* indicates Ca incorporated from the silicate-bearing minerals, # indicates by using Molecular Proportions, and indicates by using Weight Percentage).

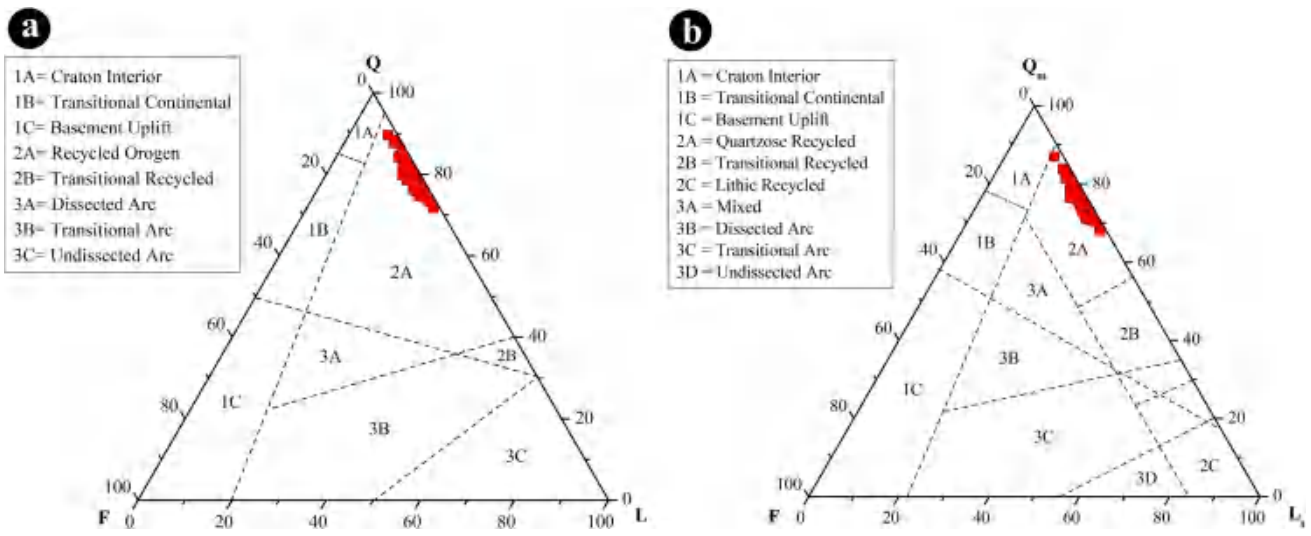

Fig. 14 Ternary plot for tectonic setting. **a** QFL plot after Dickinson and Suczek (1979), and **b** QmFLt plot after Dickinson et al. (1983) of the Barail Group of sediments

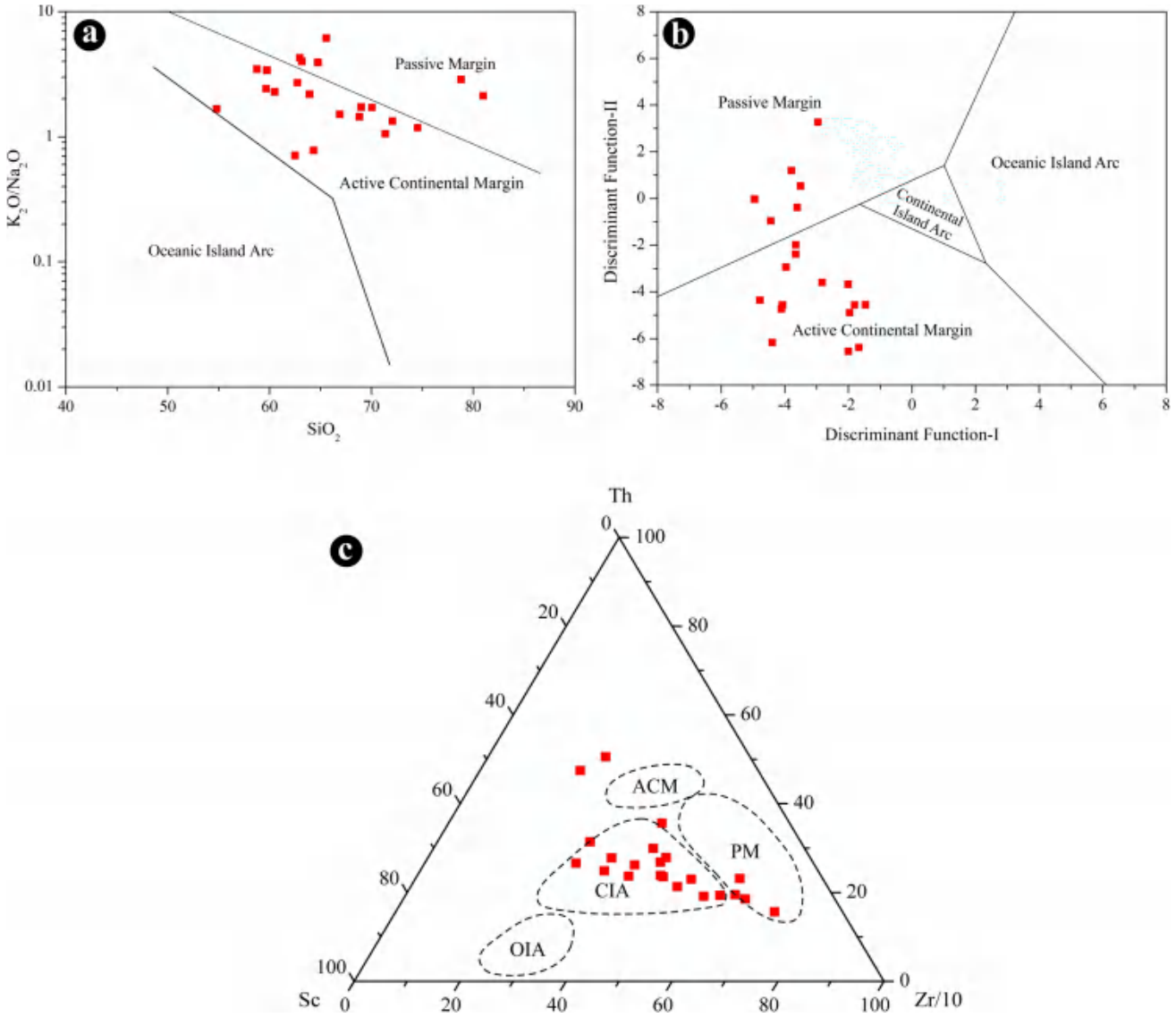

Fig. 15 Tectonic setting discrimination plot. **a** SiO_2 vs. K_2O/Na_2O bivariate tectonic setting plot after Roser and Krosch (1986), **b** Tectonic discriminant function after Bhatia (1983). (Discriminant Function-I: $(-0.0447SiO_2)$—$(0.972TiO_2)+(0.008Al_2O_3)$—$(0.267Fe_2O_3)+(0.208xFeO)$—$(3.082MnO)+(0.14MgO)+(0.195CaO)+(0.719Na_2O)$—$(0.032K_2O)+(7.51P_2O_5)+0.303$ and Discriminant Function-II: $(-0.421SiO_2)+(1.988TiO_2)$—$(0.526Al_2O_3)$—$(0.551Fe_2O_3)$—$(1.61FeO)+(2.72MnO)+(0.881MgO)$—$(0.907CaO)$—$(0.177Na_2O)$—$(1.84K_2O)+(7.244P_2O_5)+43.57$), and **c** Tectonic setting plot after Bhatia and Crook (1986) of the Barail Group of sediments. OIA-oceanic island arc; CIA-continental island arc; ACM-active continental margin; PM-passive margin

$$CIA^{\#} = \left[Al_2O_3/\left(Al_2O_3 + CaO* + Na_2O + K_2O\right)\right] \times 100$$

$$CIW^{\#} = \left[Al_2O_3/\left\{Al_2O_3 + CaO* + Na_2O\right\}\right] \times 100$$

$$WIP^{\#} = \left[\left\{2\left(Na_2O\right)/0.35\right\} + \left\{MgO/0.9\right\} + \left\{2\left(K_2O\right)/0.25\right\} + \left(CaO*/0.7\right)\right] \times 100$$

$$PIA^{\#} = \left[\left\{Al_2O_3 - K_2O\right\}/\left\{Al_2O_3 + CaO* + Na_2O - K_2O\right\}\right] \times 100$$

$$ICV^{=}[Fe_2O_3 + K_2O + Na_2O + CaO* + MgO + MnO + TiO_2/Al_2O_3]$$

The present study shows that Barail sandstones (Table S7) are moderate to a high average value of the Chemical Index of Alteration (avg. Barail: 79.14). The medium to high values of CIA indicate that the sediments traveled a distance

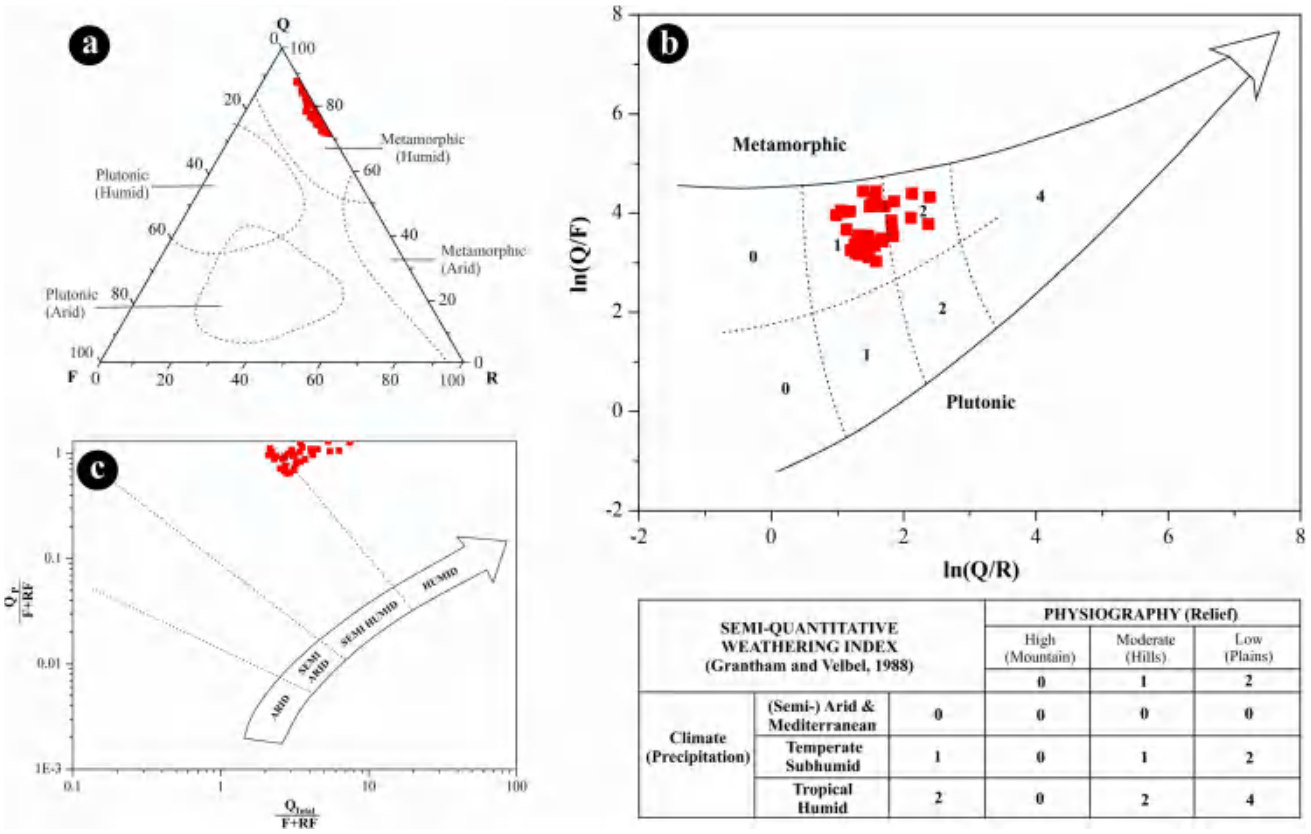

SEMI-QUANTITATIVE WEATHERING INDEX (Grantham and Velbel, 1988)			PHYSIOGRAPHY (Relief)		
			High (Mountain)	Moderate (Hills)	Low (Plains)
			0	1	2
Climate (Precipitation)	(Semi-) Arid & Mediterranean	0	0	0	0
	Temperate Subhumid	1	0	1	2
	Tropical Humid	2	0	2	4

Fig. 16 **a** QFR plot after Suttner et al. (1981), **b** Semi-Quantitative Weathering Index after Weltje 1994 and Grantham and Velbel (1988), and **c** Bivariate plot after Suttner and Dutta (1986) for climatic conditions of the Barail Group of sediments

with moderate to high mechanical breakdown and chemical change. Although the CIA is often used to evaluate weathering, the remobilization of K during sedimentation and metamorphic processes is a considerable disadvantage. Another parameter known as the CIW (Hanois 1988) is commonly used to minimize such problems. The average CIW value (86.9) indicates moderate to high weathering of the Barail sandstones, similar to PAAS (Post-Archean Australian Shale; after Taylor and McLennan 1985), i.e., 81.33. The chemical weathering intensity can also be estimated using the Plagioclase Index of Alteration (PIA, Fedo et al. 1995). Unweathered plagioclase has a PIA value of 50. The PIA values for the studied samples varied from 66.51–96.71 (avg. 85.47) (Table S7), which also justifies the above observation and resembles PAAS (77.45). The WIP values of the Barail Group (32.50) indicate moderately weathered source rocks.

In the A-CN-K ternary diagram (Nesbitt and Young 1984), the samples are almost clustered to the Al_2O_3 apex indicating moderate to highly weathered source rocks (Fig. 17a). When the weathering is low, the line follows a pattern parallel to the A-CN line. Intense weathering leaches alkalis such as CaO and Na_2O, which might cause the trend to shift towards the A-K line, suggesting K enrichment. High weathering signifies that the K has been removed and redirected the trend towards the Al_2O_3 apex. The higher values of PIA (85.47) resemble PASS (77.45) implying a supply of weathered and/or altered detritus of feldspars from the source areas as depicted in the AK-C-N plot (Fig. 17b) where samples are clustered near the AK apex. Maximum PIA value i.e. 100 indicates totally weathered products like kaolinite, gibbsite, etc., and 50 for unweathered plagioclase. The plot of CIA vs. ICV (after Long et al. 2012) represents that the source rock of the Barail Group of sediments had matured and had undergone moderate to high weathering (Fig. 17c). The binary plot of Th vs Th/U (McLennan and Hanson, 1993) is shown in Fig. 17d representing a weathering trend of the source rocks. The average value of Th/U (6.03) in the Barail sandstones shows a comparable characteristic of the upper crust that has experienced a general trend of weathering for the source rocks. (Fig. 17d).

6.7 Depositional model

Based on the field observations and lithofacies analysis a schematic depositional model has been proposed for the study area, the graphical representation of which is shown in Fig. 18.

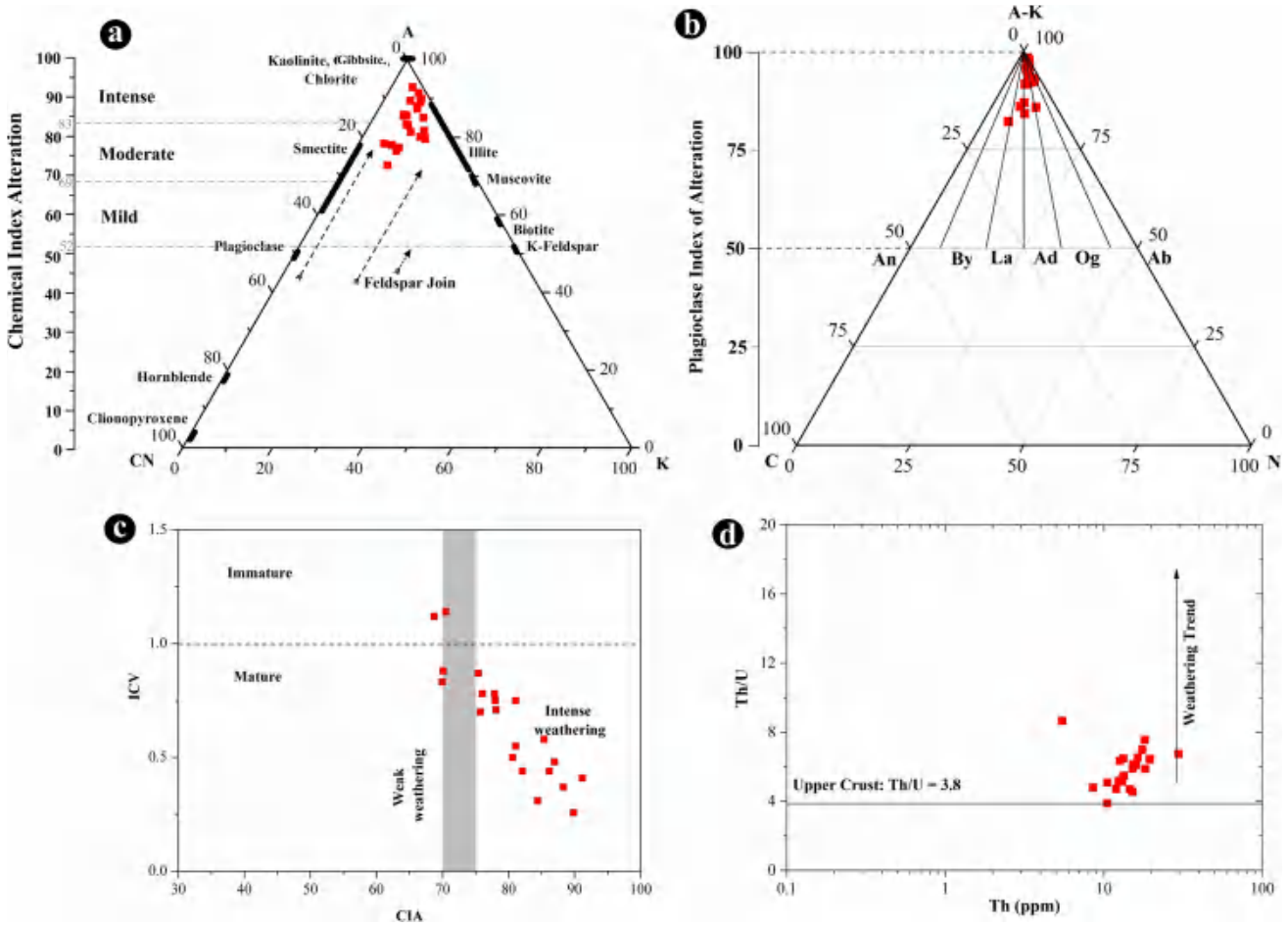

Fig. 17 **a** A-CN-K plot after Nesbitt and Young (1984) representing a moderate to intense nature of weathering of source rocks, **b** $Al_2O_3 + K_2O + Na_2O$ vs. SiO_2 plot after Suttner and Dutta (1986) for climatic condition, and **c** Binary plot of CIA vs. ICV after Long et al. (2012) representing maturity and weathering nature of the Barail Group of sediments

- **Stage 1:** During Early Paleocene time continued northward drift of the Indian Plate resulted in the initiation of subduction of the oceanic part of the Indian plate below the Tibetian plate in the north, and below the Burmese plate in the east. This caused the development of Indo-Burmese trench system, which became the locus of deposition of Disang shales under shallow to deep marine conditions.
- **Stage 2:** The continued subduction of the Indian Plate resulted in the formation of the peripheral arc system and the narrowing of the intervening sea. The Assam Shelf continued to develop in a passive margin setup. During the Oligocene period the Barail Group of sediments were deposited in a deltaic environment over the Disang Group in the basinal part.
- **Stage 3:** At the end of Oligocene, the basin was closed with total withdrawal of the sea from the basinal portion as well as from the Assam shelf. The continued push of the Indian plate on the Burmese plate after cessation of subduction, ultimately, caused westward propagation of tectonic forces, which in turn caused development of the Disang Thrust at the base of the Upper Disang shales and a number of synthetic thrusts.
- **Stage 4:** These lateral tectonic movements were accompanied by upliftment and erosion all over the shelf and in a major part of the basinal area and heralding the era of continental sedimentation, i.e., the Tipam Sandstone Formation on the Assam Shelf as well as on the earlier basinal area.
- **Stage 5:** This westward propagation of tectonic forces acting on the sediments finally resulted in the formation of numerous imbricate thrusts and upliftments which resulted in the formation of the Naga Schuppen Belt adjacent to the Assam Shelf. The Naga Thrust, a part of this thrust belt, along which the Tipam Sandstone Formation has cropped out to the surface in the study area. Towards the end of the deposition of Tipam Sandstone Formation, there was a developement of a series of N-S to NE-SW

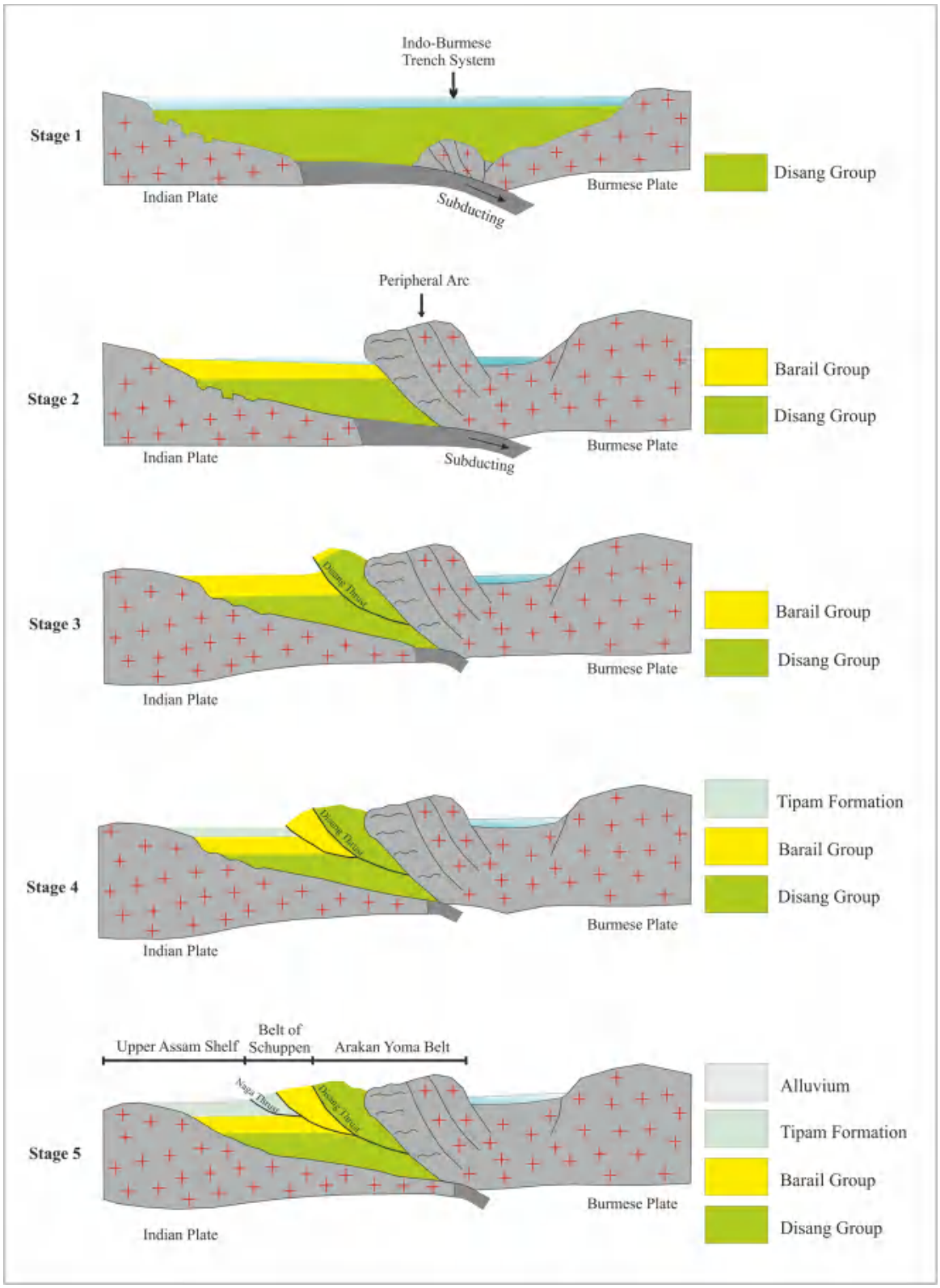

Fig. 18 A graphical representation of tectonic evolution and depositional sequences in the study area

trending compressive structures in the basinal area. During the growth of these structures, the Girujan Clay Formation was deposited in structural lows.

7 Conclusions

Based on the petrographic and whole-rock geochemical analyses of the Barail sandstones of the Belt of Schuppen, Northeast India; the following findings can be summarized:

- The Barail sandstones are mostly of sublith-arenite and litharenite types with moderate to high degree of maturity. They had undergone various diagenetic alterations after the deposition of the sediments in the basin.
- The Barail Group of sediments had been primarily sourced from the felsic to intermediate rocks of Himalayan Granitoids and their metamorphic equivalents with some contributions from the recycled sediments. The paleo-channels of the river Brahmaputra played an essential role in transporting the sediments.
- Majority of the Barail sediments have been contributed from the tectonic domains of Himalayan Ranges including: Bomi-Chayu, Gangdese Granitoid, Higher Himalayan Leucogranite and Namche Barwa with some minor contributions from ITSZ and Tethyan Leucogranite.
- The tectonic setup was active continental margin and continental island arc settings with moderate to high weathering of the source area under warm and semi-humid to humid climatic conditions before the deposition took place in the basin.

Acknowledgements We express our sincere gratitude to the Editors of Acta Geochimica for their support, guidance and editorial handling. Our special mention goes to the anonymous reviewers for their critical reviews and constructive suggestions which immensely improved the quality of the manuscript. Pradip Borgohain and Devojit Bezbaruah are grateful to the Centre of Excellence for Energy Studies (CoEES), OIL, Guwahati for extending the Financial Support to conduct the Geochemical Analysis in NGRI, Hyderabad under the Project Contract No. 6111264.

Authors contribution PB, DB and MPG designed this research work. PB, DB, MPG, YKG and GK conducted the geological field work and collected most of the field data. MPG and BB did the initial interpretation of the data and drafted the manuscript. PB, DB, YD and GRB critically analyzed the interpretations and were actively involved in the improvement of the draft. Statistical analyses of the geochemical data was conducted by AP. All the authors have participated in the discussion and contributed significantly for the improvement of this manuscript.

Declarations

Conflict of interest The authors declare that they do not have any known competing financial interests or personal relationships that could have appeared to influence the work reported in this paper.

References

Ahmad T, Tanaka T, Sachan HK, Asahara Y, Islam R, Khanna PP (2008) Geochemical and isotopic constraints on the age and origin of the Nidar Ophiolitic Complex, Ladakh, India: implications for the Neo-Tethyan subduction along the Indus suture zone. Tectonophysics 451(1–4):206–224. https://doi.org/10.1016/j.tecto.2007.11.049

Bai Y, Liu Z, Sun P, Liu R, Hu X, Zhao H, Xu Y (2015) Rare earth and major element geochemistry of Eocene fine-grained sediments in oil shale- and coal-bearing layers of the Meihe Basin northeast China. J Asian Earth Sci. 97(A):89–101. https://doi.org/10.1016/j.jseaes.2014.10.008

Armstrong-Altrin JS (2009) Provenance of sands from Cazones, Acapulco, and Bahı´a Kino beaches Mexico. Revista Mexicana de Ciencias Geologicas 26(3):764–782

Basu A, Young SW, Suttner LJ, James WC, Mack GH (1975) Re-evaluation of the use of undulatory extinction in detrital quartz for provenance interpretation. J Sediment Res. 45(4):873–882. https://doi.org/10.1306/212F6E6F-2B24-11D7-8648000102C1865D

Bédard É, Hébert R, Guilmette C, Lesage G, Wang CS, Dostal J (2009) Petrology and geochemistry of the Saga and Sangsang ophiolitic massifs, Yarlung Zangbo Suture Zone, Southern Tibet: Evidence for an arc–back-arc origin. Lithos. 113:48–67. https://doi.org/10.1016/j.lithos.2009.01.011

Bezard R, Hébert R, Wang C, Dostal J, Dai J, Zhong H (2011) Petrology and geochemistry of the Xiugugabu ophiolitic massif, western Yarlung Zangbo suture zone. Tibet Lithos. 125:347–367. https://doi.org/10.1016/j.lithos.2011.02.019

Bhatia MR (1983) Plate tectonics and geochemical composition of sandstone. J Geol. 91:611–627. https://doi.org/10.1086/628815

Bhatia MR, Crook KAW (1986) Trace element characteristics of greywackes and tectonic setting discrimination of sedimentary basins. Contrib Miner Petrol. 92:181–193. https://doi.org/10.1007/BF00375292

Bhuyan D, Borgohain P, Bezbaruah D (2022) Diagenesis and reservoir quality of Oligocene Barail Group of Upper Assam Shelf, Assam and Assam Arakan basin, India. J Asian Earth Sci X. 7:100100. https://doi.org/10.1016/j.jaesx.2022.100100

Bikramaditya RK, Chung S-L, Singh AK, Lee H-Y, Lin T-H, Iizuka Y (2020) Age and isotope geochemistry of magmatic rocks of the Lohit Plutonic Complex, eastern Himalaya: implications for the evolution of Transhimalayan arc magmatism. J Geol Soc. 177(2):379–394. https://doi.org/10.1144/jgs2018-214

Blatt H, Middleton G, Murray R (1980) Origin of sedimentary rocks. Prentice-Hall, New Jersey.

Borgohain P, Bezbaruah D, Gogoi MP, Gogoi YK, Phukan PP, Bhuyan D (2021) Petrography and diagenetic evolution of the Barail sandstones of Naga Schuppen belt, North East India: Implication towards reservoir quality. Curr Sci. 121(8):1107–1113.

Bracciali L, Marroni M, Pandolfi L, Rocchi S (2007) Geochemistry and petrography of Western Tethys Cretaceous sedimentary covers (Corsica and Northern Apennines): from source areas to configuration of margins. In: Arribas J, Critelli S, Johnsson M J (eds) Sedimentary provenance and petrogenesis: perspectives from petrography and geochemistry. Geological Society of America, Boulder. 420: 73–93. https://doi.org/10.1130/2006.2420(06)

Cao J, Wu M, Chan Y, Hu K, Bian LZ, Wang LG, Zhang Y (2012) Trace and rare earth element geochemistry of Jurassic mudstones in the northern Qaidam Basin, northwest China. Geochemistry. 72(3):245–252. https://doi.org/10.1016/j.chemer.2011.12.002

Chen L, Qin K-Z, Li G-M, Li J-X, Xiao B, Zhao J-X, Fan X (2015) Zircon U-Pb ages, geochemistry, and Sr–Nd–Pb–Hf isotopes of the Nuri intrusive rocks in the Gangdese area, southern Tibet: Constraints on timing, petrogenesis, and tectonic transformation. Lithos. 212–215:379–396. https://doi.org/10.1016/j.lithos.2014.11.014

Chen L-R, Xu W-C, Zhang H-F, Zhao P-L, Guo J-L, Luo B-J, Guo L, Pan F-B (2019a) Origin and early evolution of the Lhasa Terrane, South Tibet: constraints from the Bomi Gneiss Complex. Precambr Res. 331:105360. https://doi.org/10.1016/j.precamres.2019.105360

Chen X, Liang H, Zhang J, Sotiriou P, Huang W, Ren L, Zhang L, Zou Y (2019b) Geochemical characteristics and magma fertility for the Jurassic arc rocks in the Gangdese belt. Tibet Ore Geol Rev. 115:103169. https://doi.org/10.1016/j.oregeorev.2019.103169

Chiu HY, Chung SL, Wu FY, Liu D, Liang YH, Lin IJ, Chu MF (2009) Zircon U-Pb and Hf isotopic constraints from eastern Transhimalayan batholiths on the precollisional magmatic and tectonic evolution in southern Tibet. Tectonophysics 477(1–2):3–19. https://doi.org/10.1016/j.tecto.2009.02.034

Clark MK, Bilham R (2008) Miocene rise of the Shillong Plateau and the beginning of the end for the Eastern Himalaya. Earth and Planetary Science Letters 269(3–4):337–351. https://doi.org/10.1016/j.epsl.2008.01.045

Condie KC (1993) Chemical composition and evolution of the upper continental crust: Contrasting results from surface samples and shales. Chem Geol. 104:1–37. https://doi.org/10.1016/0009-2541(93)90140-E

Cox R, Lowe DR, Cullers RL (1995) The influence of sediment recycling and basement composition on evolution of mudrock chemistry in the southwestern United States. Geochim Cosmochim Acta. 59:2919–2940. https://doi.org/10.1016/0016-7037(95)00185-9

Critelli S, Garzanti E (1994) Provenance of the lower Tertiary Murree redbeds (Hazara-Kashmir Syntaxis, Pakistan) and initial rising of the Himalayas. Sediment Geol 89(3–4):265–284. https://doi.org/10.1016/0037-0738(94)90097-3

Cullers RL (1994) The controls on the major and trace element variation of shales, siltstones, and sandstones of Pennsylvanian-Permian age from uplifted continental blocks in Colorado to platform sediment in Kansas. USA Geochim Cosmochim Acta. 58:4955–4972. https://doi.org/10.1016/0016-7037(94)90224-0

Cullers RL (2000) The geochemistry of shales, siltstones, and sandstones of Pennsylvanian-Permian age, Colorado, USA: Implications for provenance and metamorphic studies. Lithos. 51:181–203. https://doi.org/10.1016/S0024-4937(99)00063-8

Cullers RL, Podkovyrov VN (2000) Geochemistry of the mesoproterozoic Lakhanda shales in southern Yakutia, Russia: implications for mineralogical and provenance control, and recycling. Precambr Res. 104:77–93. https://doi.org/10.1016/S0301-9268(00)00090-5

Cullers RL, Podkovyrov VN (2002) The source and origin of terrigenous sedimentary rocks in the Mesoproterozoic Ui group, southeastern Russia. Precambr Res. 117:157–183. https://doi.org/10.1016/S0301-9268(02)00079-7

Dai J, Wang C, Polat A, Santosh M, Li Y, Ge Y (2013) Rapid forearc spreading between 130 and 120Ma: evidence from geochronology and geochemistry of the Xigaze ophiolite, southern Tibet. Lithos. 172–173:1–16. https://doi.org/10.1016/j.lithos.2013.03.011

DeCelles PG, Gehrels GE, Najman Y, Martin AJ, Carter A, Garzanti E (2004) Detrital geochronology and geochemistry of Cretaceous-Early Miocene strata of Nepal: implications for timing and diachroneity of initial Himalayan orogenesis. Earth Planet Sci Lett 227(3–4):313–330. https://doi.org/10.1016/j.epsl.2004.08.019

Dickinson WR, Beard LS, Brokenridge GR, Ergavee JL, Ferguson RC, Inman KF, Knopp RA, Lindberg FA, Ryberg PT (1983) Provenance of North America Phanerozoic sandstone in relation to tectonic setting. Bull Am Geol Soc. 94:222–235. https://doi.org/10.1130/0016-7606(1983)94%3c222:PONAPS%3e2.0.CO;2

Dickinson WR, Suczek C (1979) Plate Tectonics and sandstone compositions. Bull AAPG. 63:2164–2182. https://doi.org/10.1306/2F9188FB-16CE-11D7-8645000102C1865D

Ding L (2003) Cenozoic volcanism in Tibet: evidence for a transition from oceanic to continental subduction. J Petrol. 44:1833–1865. https://doi.org/10.1093/petrology/egg061

Dong X, Peng T, Fan W, Zhao G, Zhang J, Liu B, Gao J, Peng B, Liang X, Zeng W, Chen L (2019) Origin and tectonic implications of early cretaceous high- and low-Mg series rocks and mafic enclaves in the Bomi-Chayu Fold Belt, SE Tibet. Lithos. 334–335:102–116. https://doi.org/10.1016/j.lithos.2019.03.018

Dubois-Côté V, Hébert R, Dupuis C, Wang CS, Li YL, Dostal J (2005) Petrological and geochemical evidence for the origin of the Yarlung Zangbo ophiolites, southern Tibet. Chem Geol. 214:265–286. https://doi.org/10.1016/j.chemgeo.2004.10.004

Fathy D, Wagreich M, Gier S, Mohamed RSA, Zaki R, Nady MME (2018) Maastrichtian oil shale deposition on the southern Tethys margin, Egypt: Insights into greenhouse climate and paleoceanography. Palaeogeogr Palaeoclimatol Palaeoecol. 505:18–32. https://doi.org/10.1016/j.palaeo.2018.05.017

Fedo CM, Nesbitt HW, Young GM (1995) Unravelling the effects of potassium metasomatism in sedimentary rocks and paleosols, with implications for paleoweathering conditions and provenance. Geology. 23:921–924. https://doi.org/10.1130/0091-7613(1995)023%3c0921:UTEOPM%3e2.3.CO

Folk RL (1980) Petrology of sedimentary rocks. Hemphill Publ. Co., Austin, p 182.

Fyffe LR, Pickerill RK (1993) Geochemistry of Upper Cambrian-Lower Ordovician black shale along a northeastern Appalachian transect. Geol Soc Am Bull. 105:897–910. https://doi.org/10.1130/0016-7606(1993)105%3c0897:GOUCLO%3e2.3.CO;2

Gao L-E, Zeng L, Hu G, Wang Y, Wang Q, Guo C, Hou K (2019) Early Paleozoic magmatism along the northern margin of East Gondwana. Lithos. 334–335:25–41. https://doi.org/10.1016/j.lithos.2019.03.007

Gardiner NJ, Hawkesworth CJ, Robb LJ, Whitehouse MJ, Roberts NM, Kirkland CL, Evans NJ (2017) Contrasting granite metallogeny through the zircon record: a case study from Myanmar. Sci Rep. https://doi.org/10.1038/s41598-017-00832-2

Gazzi P (1966) Le arenarie del flysch Sopra cretaceo dell'appennino modenese; Correlazioni con il Flysch di monghidoro. Mineral Petrogr Acta. 12:69–97 (**in Spanish**).

Getaneh W (2002) Geochemistry provenance and tectonic setting of the Adigrat sandstone northern Ethiopia. J Afr Earth Sc. 35(2):185–198. https://doi.org/10.1016/S0899-5362(02)00126-4

Gogoi MP, Borgohain P, Gogoi YK, Bezbaruah D (2023) Petrography, diagenesis and hydrocarbon source potential of the Barail and Disang Group of rocks in parts of the Naga Schuppen Belt and inner fold belt of Assam-Arakan Basin. J Geol Soc India. 99:906–916. https://doi.org/10.1007/s12594-023-2412-z

Grantham JH, Velbel MA (1988) The influence of climate and topography on rock-fragment abundance in modern fluvial sands of the southern Blue Ridges mountains, North Carolina. J Sediment Petrol. 58:219–227.

Guilmette C, Hébert R, Wang C, Villeneuve M (2009) Geochemistry and geochronology of the metamorphic sole underlying the

Xigaze Ophiolite, Yarlung Zangbo Suture Zone, South Tibet. Lithos. 112:149–162. https://doi.org/10.1016/j.lithos.2009.05.027

Guillot S, Garzanti E, Baratoux D, Marquer D, Mahéo G, de Sigoyer J (2003) Reconstructing the total shortening history of the NW Himalaya. Geochem Geophys Geosyst. https://doi.org/10.1029/2002GC000484

Guo L, Liu Y, Liu S, Cawood PA, Wang Z, Liu H (2013) Petrogenesis of Early to Middle Jurassic granitoid rocks from the Gangdese belt, Southern Tibet: Implications for early history of the Neo-Tethys. Lithos. 179:320–333. https://doi.org/10.1016/j.lithos.2013.06.011

Guo L, Zhang H-F, Harris N, Luo B-J, Zhang W, Xu WC (2019) Tectonic erosion and crustal relamination during the India-Asian continental collision: Insights from Eocene magmatism in the southeastern Gangdese belt. Lithos. 105161:346–347. https://doi.org/10.1016/j.lithos.2019.105161

Guo L, Zhang H-F, Harris N, Pan F-B, Xu W-C (2011) Origin and evolution of multi-stage felsic melts in eastern Gangdese belt: Constraints from U-Pb zircon dating and Hf isotopic composition. Lithos. 127:54–67. https://doi.org/10.1016/j.lithos.2011.08.005

Haproff PJ, Zuza AV, Yin A, Harrison TM, Manning CE, Dubey CS, Ding L, Wu C, Chen J (2019) Geologic framework of the northern Indo-Burma Ranges and lateral correlation of Himalayan-Tibetan lithologic units across the eastern Himalayan syntaxis. Geosphere. https://doi.org/10.1130/GES02054.1

Harnois L (1988) The CIW Index: A new chemical index of weathering. Sed Geol. 55(3–4):319–322. https://doi.org/10.1016/0037-0738(88)90137-6

Harrison TM, Yin A, Grove M, Lovera OM, Ryerson FJ, Zhou X (2000) The Zedong window: A record of superposed Tertiary convergence in southeastern Tibet. J Geophys Res 105:19211–19230. https://doi.org/10.1029/2000JB900078

Hayashi K, Fujisaw H, Holland HD, Ohmoto H (1997) Geochemistry of ~1.9 Ga sedimentary rocks from Northeastern Labrador. Canada Geochimica Cosmochimica Acta. 61:4115–4137. https://doi.org/10.1016/s0016-7037(97)00214-7

Hodges KV (2000) Tectonics of the Himalaya and southern Tibet from two perspectives. Geol Soc Am Bull 112(3):324–350

Huang C, Zhao Z, Li G, Zhu D-C, Liu D, Shi Q (2017) Leucogranites in Lhozag, southern Tibet: Implications for the tectonic evolution of the eastern Himalaya. Lithos. 294–295:246–262. https://doi.org/10.1016/j.lithos.2017.09.014

Imchen W, Thong GT, Pongen T (2014) Provenance, tectonic setting and age of the sediments of the Upper Disang Formation in the Phek District, Nagaland. J Asian Earth Sci. 88:11–27. https://doi.org/10.1016/j.jseaes.2014.02.027

Ji W-Q, Wu F-Y, Liu C-Z, Zhang H (2017) Zircon U-Pb geochronology and Hf isotopes of granitic rocks and river sands in the Nyingchi region, Tibet: Constraints on evolution of the deep crust beneath the southeast Lhasa terrane. J Asian Earth Sci. 145:613–625. https://doi.org/10.1016/j.jseaes.2017.07.006

Jiang Z, Wang Q, Wyman DA, Shi X, Yang J, Mal Gou G (2015) Zircon U-Pb geochronology and geochemistry of Late Cretaceous–early Eocene granodiorites in the southern Gangdese batholith of Tibet: Petrogenesis and implications for geodynamics and Cu Au Mo mineralization. Int Geol Rev. 57(3):373–392.

Jin ZD, Zhang EL (2002) Paleoclimate implications of Rb/Sr ratios from lake sediments. Sci Technol Eng. 2(3):20–22 (**in Chinese with English abstract**).

Jinliang Z, Xin Z (2008) Composition and provenance of sandstones and siltstones in paleogene, huimin depression, Bohia Bay Basin, Eastern China. J China Univ Geosci. 19(3):252–270. https://doi.org/10.1016/S1002-0705(08)60044-8

Kent WN, Dasgupta U (2004) Structural evolution in response to fold and thrust belt tectonics in Northern Assam, a key to hydrocarbon exploration in the jaipur anticline area. Mar Pet Geol. 21(7):785–803. https://doi.org/10.1016/j.marpetgeo.2003.12.006

Kent WN, Hickman RG, Dasgupta U (2002) Application of a ramp/flat-fault model to interpretation of the Naga Thrust and possible implications for petroleum exploration along the Naga Thrust Front. AAPG Bull. 86(12):2023–2045. https://doi.org/10.1306/61EEDDF0-173E-11D7-8645-000102C1865D

Lai S-C, Zhu R-Z (2019) Petrogenesis of Early Cretaceous high-Mg# granodiorites in the northeastern Lhasa terrane, SE Tibet: Evidence for mantle-deep crustal interaction. J Asian Earth Sci. 177:17–37. https://doi.org/10.1016/j.jseaes.2019.02.021

Lerman ADI, Gat J (eds) (1989) Physics and chemistry of lakes. Springer, Berlin.

Li L, Liu Z, George SC, Sun PC, Xu Y, Meng QT, Wang KB, Wang JX (2019) Lake evolution and its influence on the formation of oil shales in the Middle Jurassic Shimengou Formation in the Tuanyushan area, Qaidam Basin. NW China Geochem. 79(1):162–177. https://doi.org/10.1016/j.geoch.2018.12.006

Liang YH, Chung SL, Liu D, Xu Y, Wu FY, Yang JH, Wang Y, Lo CH (2008) Detrital zircon evidence from Burma for reorganization of the eastern Himalayan rivers system. Am J Sci 308(4):618–638

Lin I-J, Chung S-L, Chu C-H, Lee H-Y, Gallet S, Wu G, Ji J, Zhang Y (2012) Geochemical and Sr–Nd isotopic characteristics of Cretaceous to Paleocene granitoids and volcanic rocks, SE Tibet: Petrogenesis and tectonic implications. J Asian Earth Sci. 53:131–150. https://doi.org/10.1016/j.jseaes.2012.03.010

Liu Z-C, Wu F-Y, Ding L, Liu X-C, Wang J-G, Ji W-Q (2016) Highly fractionated Late Eocene (~35 Ma) leucogranite in the Xiaru Dome, Tethyan Himalaya, South Tibet. Lithos. 240–243:337–354. https://doi.org/10.1016/j.lithos.2015.11.026

Liu Z-C, Wu F-Y, Ji W-Q, Wang J-G, Liu C-Z (2014) Petrogenesis of the Ramba leucogranite in the Tethyan Himalaya and constraints on the channel flow model. Lithos. 208–209:118–136. https://doi.org/10.1016/j.lithos.2014.08.022

Long X, Yuan C, Sun M, Safonova I, Xiao W, Wang Y (2012) Geochemistry and U-Pb detrital zircon dating of Paleozoic graywackes in East Junggar, NW China: Insights into subduction–accretion processes in the southern Central Asian Orogenic Belt. Gondwana Res. 21:637–653. https://doi.org/10.1016/j.gr.2011.05.015

Ma M, Lei C, Rahman MJJ (2023) Paleoenvironmental reconstruction of the Eocene sediments in the Baiyun sag of the Pearl River Mouth Basin. Front Earth Sci. 11:1177240. https://doi.org/10.3389/feart.2023.1177240

Ma S, Meng Y, Xu Z, Liu X (2017) The discovery of late Triassic mylonitic granite and geologic significance in the middle Gangdese batholiths, southern Tibet. J Geodyn. 104:49–64. https://doi.org/10.1016/j.jog.2016.10.007

Mathur LP, Evans P (1964) Oil in India. In: International geological congress. 22nd Session India. 85.

McLennan SM, Hemming S, McDaniel DK, Hanson GN (1993) Geochemical approaches to sedimentation, provenance, and tectonics. Geol Soc Am Spec Pap. 284:21–40. https://doi.org/10.1130/SPE284-p21

McLennan SM, Taylor SR, McCulloch MT, Maynard JB (1990) Geochemical and Nd-Sr isotopic composition of deep-sea turbidites: Crustal evolution and plate tectonic associations. Geochim Cosmochim Acta. 54:2015–2050. https://doi.org/10.1016/0016-7037(90)90269-Q

Meng Y, Dong H, Cong Y, Xu Z, Cao H (2016) The early-stage evolution of the Neo-Tethys Ocean: evidence from granitoids in the middle Gangdese batholith, southern Tibet. J Geodyn. 94–95:34–49. https://doi.org/10.1016/j.jog.2016.01.003

Moiya JN, Luirei K, Longkumer L, Kothyari GC, Thong GT (2019) Late Quaternary deformation in parts of the Belt of Schuppen of

Dimapur and Perendistricts, Nagaland, NE India. Geol J. https://doi.org/10.1002/gj.3413
Mongelli G, Critelli S, Perri F, Sonnino M, Perrone V (2006) Sedimentary recycling, provenance and paleoweathering from chemistry and mineralogy of Mesozoic continental red bed mud rocks, Peloritani mountains, southern Italy. Geochem J 40:197–209. https://doi.org/10.2343/geochemj.40.197
Moradi VA, Sari A, Akkaya P (2016) Geochemistry of the Miocene oil shale (Hançili Formation) in the Çankırı-Çorum Basin, Central Turkey: implications for Paleoclimate conditions, source–area weathering, provenance and tectonic setting. Sed Geol. 341:289–303. https://doi.org/10.1016/j.sedgeo.2016.05.002
Morley CK, Searle M (2017) Regional tectonics, structure and evolution of the Andaman Nicobar Islands from ophiolite formation and obduction to collision and back–arc spreading. Geol Soc Lond Mem 47:51–74. https://doi.org/10.1144/M47.5
Najman Y, Bracciali L, Parrish RR, Chisty E, Copley A (2016) Evolving strain partitioning in the Eastern Himalaya: the growth of the Shillong Plateau. Earth Planet Sci Lett 433:1–9. https://doi.org/10.1016/j.epsl.2015.10.017
Nesbitt HW, Fedo CM, Young GM (1997) Quartz and feldspar stability, steady and non-steady-state weathering and petrogenesis of siliciclastic sands and muds. J Geol. 105:173–191. https://doi.org/10.1086/515908
Nesbitt HW, Young GM (1982) Early Proterozoic climates and plate motions inferred from major element chemistry of lutites. Nature. 299:715–717. https://doi.org/10.1038/299715a0
Nesbitt HW, Young GM (1984) Prediction of some weathering trends of plutonic and volcanic rocks based on thermodynamic and kinetic considerations. Geochim Cosmochim Acta. 48:1523–1534. https://doi.org/10.1016/0016-7037(84)90408-3
Nesbitt HW, Young GM, McLennan SM, Keays RR (1996) Effect of geochemical weathering and sorting on the petrogenesis of siliciclastic sediments, with implications for provenance studies. J Geol. 104:525–542. https://doi.org/10.1086/629850
Pan F-B, Zhang H-F, Harris N, Xu W-C, Guo L (2012) Oligocene magmatism in the eastern margin of the east Himalayan syntaxis and its implication for the India-Asia post-collisional process. Lithos. 154:181–192. https://doi.org/10.1016/j.lithos.2012.07.004
Parker A (1970) An index of weathering for silicate rocks. Geol Mag. 107:501–504. https://doi.org/10.1017/S0016756800058581
Pettijohn FJ, Potter PE, Siever R (1972) Sand and sandstones. Springer, New York.
Pivnik DA, Wells NA (1996) The transition from Tethys to the Himalaya as recorded in northwest Pakistan. Geol Soc Am Bull 108(10):1295–1313
Ranga RA, Murthy KN (1969) On the origin of Naga thrust. Naga Hills Bull ONGC. 6(2):51–56.
Rao AR (1983) Geology and hydrocarbon potential of a part of Assam-Arakan Basin and its adjacent regions. Petrol Asia J 6(4):127–158
Reichardt H, Weinberg RF, Andersson UB, Fanning CM (2010) Hybridization of granitic magmas in the source: the origin of the Karakoram Batholith, Ladakh NW India. Lithos 116(3–4):249–272. https://doi.org/10.1016/j.lithos.2009.11.013
Roser BP, Korsch RJ (1986) Determination of tectonic setting of sandstone-mudstone suites using SiO_2 content and K_2O/Na_2O ratio. J Geol. 94:635–650. https://doi.org/10.1086/629071
Roser BP, Korsch RJ (1988) Provenance signatures of sandstone-mudstone suites determined using discriminant function analysis of major-element data. Chem Geol. 67:119–139. https://doi.org/10.1016/0009-2541(88)90010-1
Rowley DB (1996) Age of initiation of collision between India and Asia: a review of stratigraphic data. Earth Planet Sci Lett 145(1–4):1–13. https://doi.org/10.1016/S0012-821X(96)00201-4
Rudnick RL, Gao S (2003) 3.01 - Composition of the continental crust. Treat Geochem. 3:1–64. https://doi.org/10.1016/B0-08-043751-6/03016-4
Samad SK, Mishra DK, Mathews RP, Ghosh S, Mendhe VA, Varma AK (2020) Geochemical attributes for source rock and palaeoclimatic reconstruction of the Auranga Basin, India. J Petrol Sci Eng. 185:106665. https://doi.org/10.1016/j.petrol.2019.106665
Satyanarayanan M, Balaram V, Sawant SS, Subramanyam KSV, Vamsi Krishna G, Dasaram B, Manikyamba C (2018) Rapid determination of REEs, PGEs, and other trace elements in geological and environmental materials by high resolution inductively coupled plasma mass spectrometry. At Spectrosc. 39(1):1–15.
Schoenborn WA, Fedo C (2011) Provenance and paleoweathering reconstruction of the Neoproterozoic Johnnie formation, southeastern California. Chem Geol. 285:231–255. https://doi.org/10.1016/j.chemgeo.2011.04.014
Srivastava SK, Pandey N (2011) Search for provenance of oligocene Barail sandstones in and around Jotsoma, Kohima, Nagaland. J Geol Soc India. 77:433–442. https://doi.org/10.1007/s12594-011-0045-0
Suttner LJ, Basu A, Mach GH (1981) Climate and the origin of Quartz arenites. J Sediment Petrol. 51:1235–1246.
Suttner LJ, Dutta PK (1986) Alluvial sandstone composition and paleoclimate framework mineralogy. J Sediment Petrol. 56(3):329–345.
Tao S, Xu Y, Tang D, Xu H, Li S, Chen S, Liu W, Cui Y, Gou M (2017) Geochemistry of the Shitoumei oil shale in the Santanghu Basin, Northwest China: Implications for paleoclimate conditions, weathering, provenance and tectonic setting. Int J Coal Geol. 184:42–56. https://doi.org/10.1016/j.coal.2017.11.007
Taylor SR, McLennan SM (1985) The Continental crust: Its composition and evolution. Blackwell Scientific, Oxford, p 312.
Thong GT, Rao BV (1999) Petrochemical studies of the Barail sediments of Botsa, Kohima District, Nagaland. J Indian Acad Geosci. 42:32–37.
Tian S, Hou Z, Chen X, Tian H, Gong Y, Yang Z, Huang T, Li X, Mo X (2020) Magnesium isotopic behaviors between metamorphic rocks and their associated leucogranites, and implications for Himalayan orogenesis. Gondwana Res. 87:23–40. https://doi.org/10.1016/j.gr.2020.06.006
Tian S, Zhao Y, Hou Z, Tian Y, Hou K, Li X, Yang Z, Hu W, Mo X, Zheng Y (2017) Lithium isotopic composition and concentration of Himalayan leucogranites and the Indian lower continental crust. Lithos. 284–285:416–428. https://doi.org/10.1016/j.lithos.2017.05.001
Tortosa A, Palomares M, Arribas J (1991) Quartz grain types in Holocene deposits from the Spanish Central System: Some problems in provenance analysis. Geol Soc London Spe Publ. 57:47–54. https://doi.org/10.1144/GSL.SP.1991.057.01.05
Uddin A, Lundberg N (1999) A paleo-brahmaputra? Subsurface lithofacies analysis of miocene deltaic sediments in the Himalayan-Bengal system. Bangl Sediment Geol. 123:239–254. https://doi.org/10.1016/S0037-0738(98)00134-1
Visonà D (2002) Two-mica and tourmaline leucogranites from the Everest-Makalu region (Nepal–Tibet). Himalayan leucogranite genesis by isobaric heating? Lithos. 62:125–150. https://doi.org/10.1016/S0024-4937(02)00112-3
Wang C, Ding L, Zhang L-Y, Kapp P, Pullen A, Yue Y-H (2016) Petrogenesis of middle-late triassic volcanic rocks from the Gangdese belt, southern Lhasa terrane: Implications for early subduction of Neo-Tethyan oceanic lithosphere. Lithos. 262:320–333. https://doi.org/10.1016/j.lithos.2016.07.021
Wang Q, Zhu D-C, Cawood PA, Zhao Z-D, Liu S-A, Chung S-L, Zhang L-L, Liu D, Zheng Y-C, Dai J-G (2015) Eocene magmatic processes and crustal thickening in southern Tibet: insights from strongly fractionated ca. 43 Ma granites in the western Gangdese

Batholith. Lithos. 239:128–141. https://doi.org/10.1016/j.lithos.2015.10.003

Wang X, Liu W, Zhong Y, Hu X, Xia B, Huang W (2018) Geochemical and zircon U-Pb age constraints on the origin of the Mesozoic Xigaze ophiolite, Yarlung Zangbo suture zone SW China. Int Geol Rev. 60:1267–1289. https://doi.org/10.1080/00206814.2017.1385034

Weltje GJ (1994) Provenance and dispersal of sand-sized sediments: reconstruction of dispersal patterns and sources of sand-sized sediments by means of inverse modelling techniques (Ph.D. thesis). Utrecht University Geologica Ultraiectina. 121.

Wronkiewicz DJ, Condie KC (1987) Geochemistry of archean shales from the witwatersr and supergroup, South Africa: Source-area weathering and provenance. Geochim Cosmochim Acta. 51:2401–2416. https://doi.org/10.1016/0016-7037(87)90293-6

Wu Y, Liu C, Liu Y, Gong H, Awan RS, Li G, Zang Q (2022) Geochemical characteristics and the organic matter enrichment of the Upper Ordovician Tanjianshan Group, Qaidam Basin, China. J Pet Sci Eng. 208(1):109383. https://doi.org/10.1016/j.petrol.2021.109383

Xiao L, He Q, Pirajno F, Ni P, Du J, Wei Q (2008) Possible correlation between a mantle plume and the evolution of Paleo-Tethys Jinshajiang Ocean: Evidence from a volcanic rifted margin in the Xiaru-Tuoding area, Yunnan, SW China. Lithos. 100:112–126. https://doi.org/10.1016/j.lithos.2007.06.020

Xie Z, Xue C, Yang T, Xiang K, Xin D (2020) Petrogenesis and geodynamic implications of early cretaceous highly fractionated leucogranites in the northern Lanping-Simao terrane, Eastern Tibetan Plateau. J Asian Earth Sci. 197:104340. https://doi.org/10.1016/j.jseaes.2020.104340

Xu W-C, Zhang H-F, Harris N, Guo L, Pan F-B, Wang S (2013) Geochronology and geochemistry of Mesoproterozoic granitoids in the Lhasa terrane, south Tibet: Implications for the early evolution of Lhasa terrane. Precambr Res. 236:46–58. https://doi.org/10.1016/j.precamres.2013.07.016

Xu W-C, Zhang H-F, Luo B, Guo L, Yang H (2015) Adakite-like geochemical signature produced by amphibole-dominated fractionation of arc magmas: An example from the Late Cretaceous magmatism in Gangdese belt, south Tibet. Lithos. 232:197–210. https://doi.org/10.1016/j.lithos.2015.07.001

Yang L, Liu X-C, Wang J-M, Wu F-Y (2019) Is Himalayan leucogranite a product by in situ partial melting of the Greater Himalayan Crystalline? A comparative study of leucosome and leucogranite from Nyalam, southern Tibet. Lithos. 342–343:542–556. https://doi.org/10.1016/j.lithos.2019.06.007

Zeng L, Gao LE, Tang S, Hou K, Guo C, Hu G (2014) Eocene magmatism in the Tethyan Himalaya, southern Tibet. Geol Soc Lond Spec Publ 412(1):287–316. https://doi.org/10.1144/SP412.8

Zeng L, Gao L-E, Tang S, Hou K, Guo C, Hu G (2015) Eocene magmatism in the Tethyan Himalaya, southern Tibet. In: Mukherjee S *et al*, (eds) Tectonics of the Himalaya. Geological Society of London, London, UK 287–316. https://doi.org/10.1144/SP412.8

Zhang H, Harris N, Guo L, Xu W (2010a) The significance of Cenozoic magmatism from the western margin of the eastern syntaxis, southeast Tibet. Contrib Mineral Petrol. 160:83–98. https://doi.org/10.1007/s00410-009-0467-5

Zhang H, Harris N, Parrish R, Kelley S, Zhang L, Rogers N, Argles T, King J (2004) Causes and consequences of protracted melting of the mid-crust exposed in the North Himalayan antiform. Earth Planet Sci Lett. 228:195–212. https://doi.org/10.1016/j.epsl.2004.09.031

Zhang Z, Dong X, Santosh M, Liu F, Wang W, Yiu F, He Z, Shen K (2012) Petrology and geochronology of the Namche Barwa Complex in the eastern Himalayan syntaxis, Tibet: constraints on the origin and evolution of the north-eastern margin of the Indian Craton. Gondwana Res. 21:123–137. https://doi.org/10.1016/j.gr.2011.02.002

Zhang Z, Dong X, Xiang H, He Z, Liou JG (2014) Metagabbros of the Gangdese arc root, south Tibet: implications for the growth of continental crust. Geochim Cosmochim Acta. 143:268–284. https://doi.org/10.1016/j.gca.2014.01.045

Zhang Z, Dong X, Xiang H, Liou JG, Santosh M (2013) Building of the deep gangdese arc, South Tibet: Paleocene plutonism and granulite-facies metamorphism. J Petrol. 54:2547–2580. https://doi.org/10.1093/petrology/egt056

Zhang Z, Zhao G, Santosh M, Wang J, Dong X, Shen K (2010b) Late Cretaceous charnockite with adakitic affinities from the Gangdese batholith, southeastern Tibet: Evidence for Neo-Tethyan mid-ocean ridge subduction? Gondwana Res. 17:615–631. https://doi.org/10.1016/j.gr.2009.10.007

Zheng H, Huang Q, Kapsiotis A, Xia B, Yin Z, Zhong Y, Lu Y, Shi X (2017) Early cretaceous ophiolites of the Yarlung Zangbo Suture Zone: Insights from dolerites and peridotites from the Baer upper mantle suite, SW Tibet (China). Int Geol Rev. 59:1471–1489. https://doi.org/10.1080/00206814.2016.1276867

Zhong Y, Liu W-L, Tang G-J, Liu N-N, Liu H-F, Zeng Q-G, Xia B (2019) Origin of Mesozoic ophiolitic mélanges in the western Yarlung Zangbo suture zone. SW Tibet Gondwana Res. 76:204–223. https://doi.org/10.1016/j.gr.2019.06.008

Zhao N, Ye J, Yang B, Zhang F, Yu H, Xu C, Xu S, Xu J, Shu Y (2021) Depositional palaeoenvironment and models of the Eocene lacustrine source rocks in the northern South China Sea. Mar Pet Geol. 128:105015. https://doi.org/10.1016/j.marpetgeo.2021.105015

Zhao ZY, Zhao JH, Wang HJ, Liao JD, Liu CM (2007) Distribution characteristics and applications of trace elements in Junggar Basin. Nat Gas Explor Dev. 30:30–33 (**in Chinese with English abstract**).

Zhou J, Yang Z, Hou Z, Liu Y, Zhao X, Zhang X, Zhao M, Ma W (2017) The geochemical evolution of syncollisional magmatism and the implications for significant magmatic-hydrothermal lead–zinc mineralization (Gangdese, Tibet). Lithos. 288–289:143–155. https://doi.org/10.1016/j.lithos.2017.07.004

Zhu D-C, Zhao Z-D, Pan G-T, Lee H-Y, Kang Z-Q, Liao Z-L, Wang L-Q, Li G-M, Dong G-C, Liu B (2009) Early cretaceous subduction-related adakite-like rocks of the Gangdese Belt, southern Tibet: Products of slab melting and subsequent melt–peridotite interaction? J Asian Earth Sci. 34:298–309. https://doi.org/10.1016/j.jseaes.2008.05.003

Zhu R-Z, Lai S-C, Qin J-F, Santosh M, Zhao S, Zhang E, Zong C, Zhang X, Xue Y (2020) Genesis of high-potassium calc-alkaline peraluminous I-type granite: new insights from the Gaoligong belt granites in southeastern Tibet Plateau. Lithos. 354–355:105343. https://doi.org/10.1016/j.lithos.2019.105343

Zhu R-Z, Lai S-C, Qin J-F, Zhao S-W, Wang J-B (2017) Late Early-Cretaceous quartz diorite–granodiorite–monzogranite association from the Gaoligong belt, southeastern Tibet Plateau: Chemical variations and geodynamic implications. Lithos. 288–289:311–325. https://doi.org/10.1016/j.lithos.2017.07.021